REPORT NO. DOT-TSC-RSPA-80-5

DYNAMIC RESPONSE OF FINITE LENGTH MAGLEV VEHICLES SUBJECTED TO CROSSWIND GUSTS

by

Devendra P. Garg
Timothy M. Barrows

U.S. Department of Transportation
Research and Special Programs Administration
Transportation Systems Center
Cambridge MA 02142

MARCH 1980
FINAL REPORT

Prepared for

U.S. DEPARTMENT OF TRANSPORTATION
RESEARCH AND SPECIAL PROGRAMS ADMINISTRATION
Office of Systems Engineering
Washington DC 20590

Technical Report Documentation Page

1. Report No.	2. Government Accession No.	3. Recipient's Catalog No.
DOT-TSC-RSPA-80-5		

4. Title and Subtitle	5. Report Date
DYNAMIC RESPONSE OF FINITE LENGTH MAGLEV VEHICLES SUBJECTED TO CROSSWIND GUSTS	March 1980
	6. Performing Organization Code
7. Author(s)	8. Performing Organization Report No.
Devendra P. Garg, Timothy M. Barrows	DOT-TSC-RSPA-80-5
9. Performing Organization Name and Address	10. Work Unit No. (TRAIS)
U.S. Department of Transportation Research and Special Programs Administration Transportation Systems Center Cambridge MA 02142	RS033/R0545
	11. Contract or Grant No.
12. Sponsoring Agency Name and Address	13. Type of Report and Period Covered
U.S. Department of Transportation Research and Special Programs Administration Office of Systems Engineering Washington DC 20590	Final Report June-September 1979
	14. Sponsoring Agency Code
	DPB-25

15. Supplementary Notes

16. Abstract

A two-degree-of-freedom model for magnetically levitated finite length vehicles incorporating sway and yaw dynamics is formulated. Aerodynamic lateral forces and yawing moments on the vehicle resulting from constant speed wind gusts are computed using analytical techniques. Computer simulations are run for three vehicle speeds and three apparent mass factors. It is shown that higher apparent mass factors can be instrumental in reducing peak displacements and acceleration levels. The guidance-to-lift ratio is not as much affected by an increase in apparent mass factor as are the displacements and accelerations.

17. Key Words	18. Distribution Statement
Ground Vehicle Aerodynamics, Crosswind Aerodynamics, Magnetic Levitation, High Speed Ground Transportation, Non-contact Suspensions	DOCUMENT IS AVAILABLE TO THE PUBLIC THROUGH THE NATIONAL TECHNICAL INFORMATION SERVICE, SPRINGFIELD, VIRGINIA 22161

19. Security Classif. (of this report)	20. Security Classif. (of this page)	21. No. of Pages	22. Price
UNCLASSIFIED	UNCLASSIFIED	62	

Form DOT F 1700.7 (8-72) Reproduction of completed page authorized

PREFACE

This work was performed in support of the Non-Contact Suspension and Propulsion Program of the Office of Systems Engineering (OSE) in the Research and Special Programs Administration (RSPA).

One objective of this program is to maintain a sufficient level of U.S. effort in this technology to keep abreast of developments in Japan and Germany, both of which are building full-scale test tracks for speeds of 400 km/hr and above. The aerodynamic side-gust problem is of considerable interest at these speeds, and it leads naturally to questions of vehicle ride quality for which there exists a related program of active cooperation between Germany and the U.S.

Professor Devendra P. Garg of Duke University made the major contribution to this report while he was with the Advanced Systems Branch of the Transportation Systems Center (TSC) on a Faculty Fellowship Program during the summer of 1979. Dr. Timothy M. Barrows is a full-time employee of TSC, and has been active in non-contact suspension research since 1965.

The constant encouragement of Mr. Lawrence P. Greene, Branch Chief, through all phases of this research is gratefully acknowledged. Thanks are also due to Professor David N. Wormley of MIT for providing valuable technical information, and to Mr. Harvey Lee and Gary Watros of TSC for providing basic information on the TSC computing system.

METRIC CONVERSION FACTORS

Approximate Conversions to Metric Measures

Symbol	When You Know	Multiply by	To Find	Symbol
		LENGTH		
in	inches	2.5	centimeters	cm
ft	feet	30	centimeters	cm
yd	yards	0.9	meters	m
mi	miles	1.6	kilometers	km
		AREA		
in^2	square inches	6.5	square centimeters	cm^2
ft^2	square feet	0.09	square meters	m^2
yd^2	square yards	0.8	square meters	m^2
mi^2	square miles	2.6	square kilometers	km^2
	acres	0.4	hectares	ha
		MASS (weight)		
oz	ounces	28	grams	g
lb	pounds	0.45	kilograms	kg
	short tons (2000 lb)	0.9	tonnes	t
		VOLUME		
tsp	teaspoons	5	milliliters	ml
Tbsp	tablespoons	15	milliliters	ml
fl oz	fluid ounces	30	milliliters	ml
c	cups	0.24	liters	l
pt	pints	0.47	liters	l
qt	quarts	0.95	liters	l
gal	gallons	3.8	liters	l
ft^3	cubic feet	0.03	cubic meters	m^3
yd^3	cubic yards	0.76	cubic meters	m^3
		TEMPERATURE (exact)		
°F	Fahrenheit temperature	5/9 (after subtracting 32)	Celsius temperature	°C

Approximate Conversions from Metric Measures

Symbol	When You Know	Multiply by	To Find	Symbol
		LENGTH		
mm	millimeters	0.04	inches	in
cm	centimeters	0.4	inches	in
m	meters	3.3	feet	ft
m	meters	1.1	yards	yd
km	kilometers	0.6	miles	mi
		AREA		
cm^2	square centimeters	0.16	square inches	in^2
m^2	square meters	1.2	square yards	yd^2
km^2	square kilometers	0.4	square miles	mi^2
ha	hectares (10,000 m^2)	2.5	acres	
		MASS (weight)		
g	grams	0.035	ounces	oz
kg	kilograms	2.2	pounds	lb
t	tonnes (1000 kg)	1.1	short tons	
		VOLUME		
ml	milliliters	0.03	fluid ounces	fl oz
l	liters	2.1	pints	pt
l	liters	1.06	quarts	qt
l	liters	0.26	gallons	gal
m^3	cubic meters	35	cubic feet	ft^3
m^3	cubic meters	1.3	cubic yards	yd^3
		TEMPERATURE (exact)		
°C	Celsius temperature	9/5 (then add 32)	Fahrenheit temperature	°F

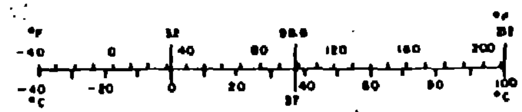

TABLE OF CONTENTS

LIST OF ILLUSTRATIONS

LIST OF ILLUSTRATIONS (CONT.)

LIST OF TABLES

SYMBOLS AND ABBREVIATIONS

b	damping constant for magnetic suspension
b_y	suspension damping in sway mode
b_ψ	suspension damping in yaw mode
C_n	yawing moment coefficient
C_y	aerodynamic force coefficient
$C_{n_{fs}}$	yawing moment coefficient due to slender body part
C_{n_c}	yawing moment coefficient due to viscous cross flow
$C_{y_{fs}}$	side force coefficient due to slender body part
C_{y_c}	side force coefficient due to viscous cross flow
F	suspension lateral force
F_{aero}	aerodynamic side force
$f(t)$	general time-dependent function
$g(\sigma)$	modified-Bryson function
H_v	maximum height of vehicle
I	vehicle moment of inertia
I_a	apparent moment of inertia for vehicle
k	configuration factor
K	stiffness of magnetic suspension
k_1, k_2, k_3	slopes of linear segments for force and moment curves
k_y	suspension stiffness in sway mode
k_ψ	suspension stiffness in yaw mode

ℓ	location of magnetic suspension block from center
ℓ_1	length of nose section
ℓ_v	vehicle half length
m	vehicle mass
m_a	apparent mass of vehicle
M_z	aerodynamic torque on the vehicle
q	dynamic pressure = $\frac{1}{2} \rho V_r^2$
s	Laplace Operator
S	reference area presented to wind gust = $(\pi/2) H_v^2$
t	time following gust entry
T_1, T_2, T_3	break point values of time t in approximation curves
V	vehicle velocity
V_c	velocity of cross wind gust
V_r	relative velocity of wind gust
W	vehicle weight
w	nondimensional parameter, $\frac{Vt}{\ell_1}$
y	sway displacement
$y_1,...,y_4$	state variables in dynamic equations
z	nondimensional parameter, Vt/ℓ_v
β	side-slip angle = $\tan^{-1} (V_c/V)$
ζ_y	damping ratio in sway mode
ζ_ψ	damping ratio in yaw mode

λ	linear ratio ℓ_v/H_v
λ_1	linear ratio ℓ_1/H_v
ρ	air density
σ	parameter in modified-Bryson function
ψ	yaw displacement
ω_y	natural frequency in sway mode
ω_ψ	natural frequency in yaw mode

1. INTRODUCTION

In recent years much emphasis has been in evidence on research and development of non-contact suspensions for tracked-levitated vehicles [1-5].* Advanced suspension concepts are necessary to provide the desired degree of passenger comfort and acceptable levels of ride quality. Fluid and attractive and repulsive magnetic suspensions have been considered in both the USA and abroad [6-9] for this purpose. The main focus of the present paper is on attractive ferromagnetic suspension, which can operate with low noise levels, low pollution, and reasonable energy efficiency [10].

Several reports and technical papers [11-22] have addressed the problem of ferromagentic suspensions. Basically, there are two types of magnetic suspensions currently under development and further investigation [23]. One is the "repulsive" type in which superconducting magnets are used on board. These magnets, in conjunction with vehicle forward speed, produce eddy currents in the conducting guideway, and thus produce levitation by repulsion. Since there is no lift while stationary, the vehicle is supported by wheels at low speeds. Initially, the lift force increases with an increase in speed and finally levels-off at lift off speeds of 40-80 mi/hr [22]. The typical gap sizes and operating speeds are, respectively, 4-8 inches and 180-300 mi/hr.

*Numbers in square brackets designate Reference items at the end of text in this report.

In the "attractive" concept, conventional electromagnets, located on the vehicle, are suspended below a steel track, thus providing an attractive force between the track and the vehicle. Since the configuration is inherently unstable, the position of the magnets relative to the track is monitored on a continuous basis and active feedback control is employed to insure stability. The suspension achieves its maximum lift at zero speed, and at higher speeds the lift force is degraded due to generation of eddy currents in the track. In order to operate with a reasonable amount of power, the nominal gap is maintained at a much smaller value than the "repulsion" type of suspension. In general, the operating speeds are also lower in this case. Typical range of nominal gap values is 0.4-0.8 in.

In addition to levitation, guidance is also provided by the magnets. In one configuration, separate magnets are used for vertical support and lateral guidance. The levitation and guidance forces are essentially normal to the pole faces. In another configuration, simultaneous lift and guidance functions are provided by both primary and fringing fields [22]. The forces are tangential and normal to the pole faces in this case, and an inverted U-shaped rail is used instead of a flat rail. The control strategy used for this configuration requires that the magnet pairs are staggered relative to rail centerline so that lift and guidance forces may be controlled independently (see Figure 1-1).

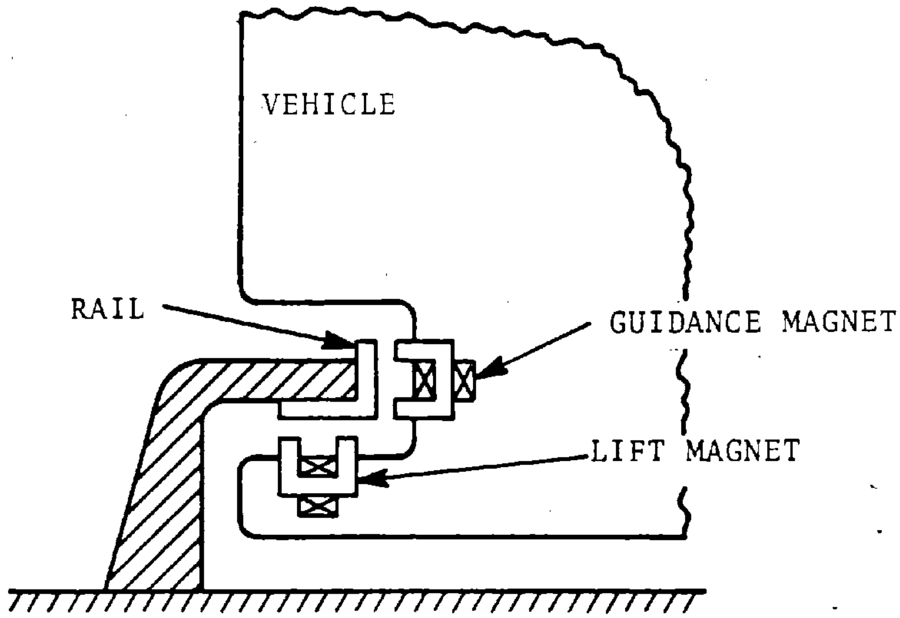

a) SEPARATE LIFT AND GUIDANCE

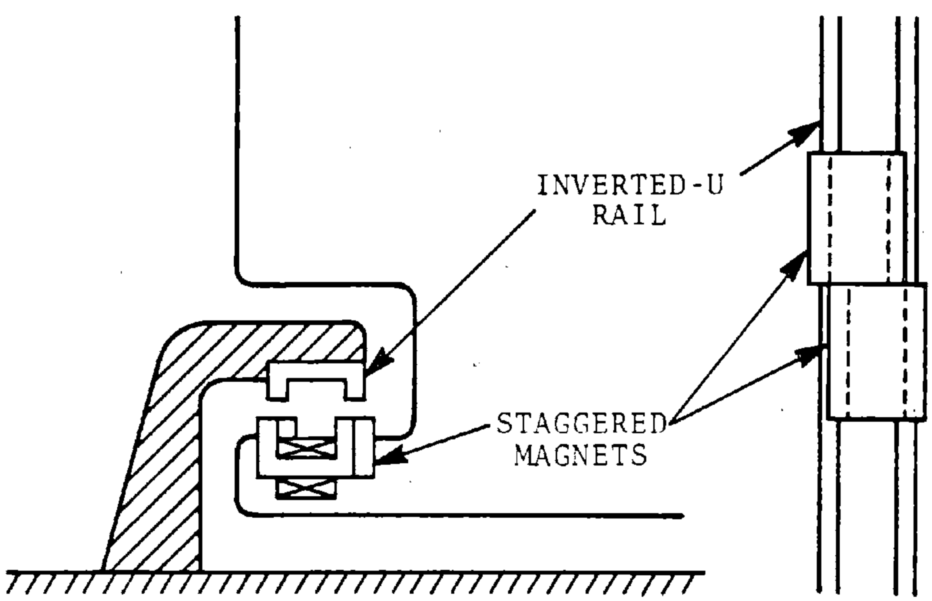

b) COMBINED LIFT AND GUIDANCE

FIGURE 1-1. CANDIDATE CONFIGURATIONS FOR GUIDANCE USING FERROMAGNETIC SUSPENSION

The work reported in Reference 4 examines the relative advantages of combined versus separate lift and guidance. It was found that for a guidance-to-lift ratio in the range of 0.5, combining the lift and guidance functions into one set of magents results in a system which is about 20 percent lighter than a system using separate magnets. For higher guidance-to-lift ratios the separate system tends to become advantageous, whereas for lower ratios the advantage of combined magnets becomes greater. Thus there is a particular interest in determining just what guidance force capability is required from a magnetic suspension. The present study of aerodynamic gust response is primarily motivated by this issue.

Some research has gone into aerodynamic side gust forces of ground vehicles [24, 25] and wind tunnel tests have been conducted on scaled-down models.

This report deals with dynamic modeling and response of magnetically levitated vehicles entering aerodynamic side gust fields. A two-degree-of-freedom dynamic model is formulated and computation of dynamic forces and moments is shown for three different vehicle speeds. Piecewise straight line approximations are used for representation of both force and moment curves in computer simulations. Peak displacement, acceleration and guidance-to-lift ratio are computed for three vehicle speeds. Results are discussed and recommendations are made for further work.

1.1 VEHICLE DYNAMIC MODEL

The vehicle model considered in this report is a two-degree-of-freedom system, in which both sway and yaw motions are included. The model represents a finite length vehicle shown in Figure 1. The vehicle is assumed to act as a rigid body with a uniform mass distribution. Length of the vehicle is 2 ℓ_V and the suspension magnets are assumed to be located at a distance of ℓ on either end of the center. Nose length of the vehicle is ℓ_1. The symbol y denotes the sway motion, and ψ represents yaw.

The vehicle, traveling at a velocity of V, penetrates a region containing a stationary crosswind gust of velocity V_c, as shown in Figure 1-2. The model is assumed to be decoupled in the yaw and sway modes. This assumption is justified in view of the use of active control for vehicle suspensions[26]. In the present analysis it is assumed that a linear control law incorporating position, velocity and acceleration feedback is used leading to an increase in the vehicles' effective mass and a minimization of the yaw-sway coupling [27]. Also, with this control strategy an arbitrary natural frequency and damping ratio can be chosen by using appropriate values of controller gains.

1.2 EQUATION OF MOTION

The vehicle is assumed to be subjected to aerodynamic crosswind gust loading while travelling at a constant vehicle of V mi /hr Since this analysis is primarily

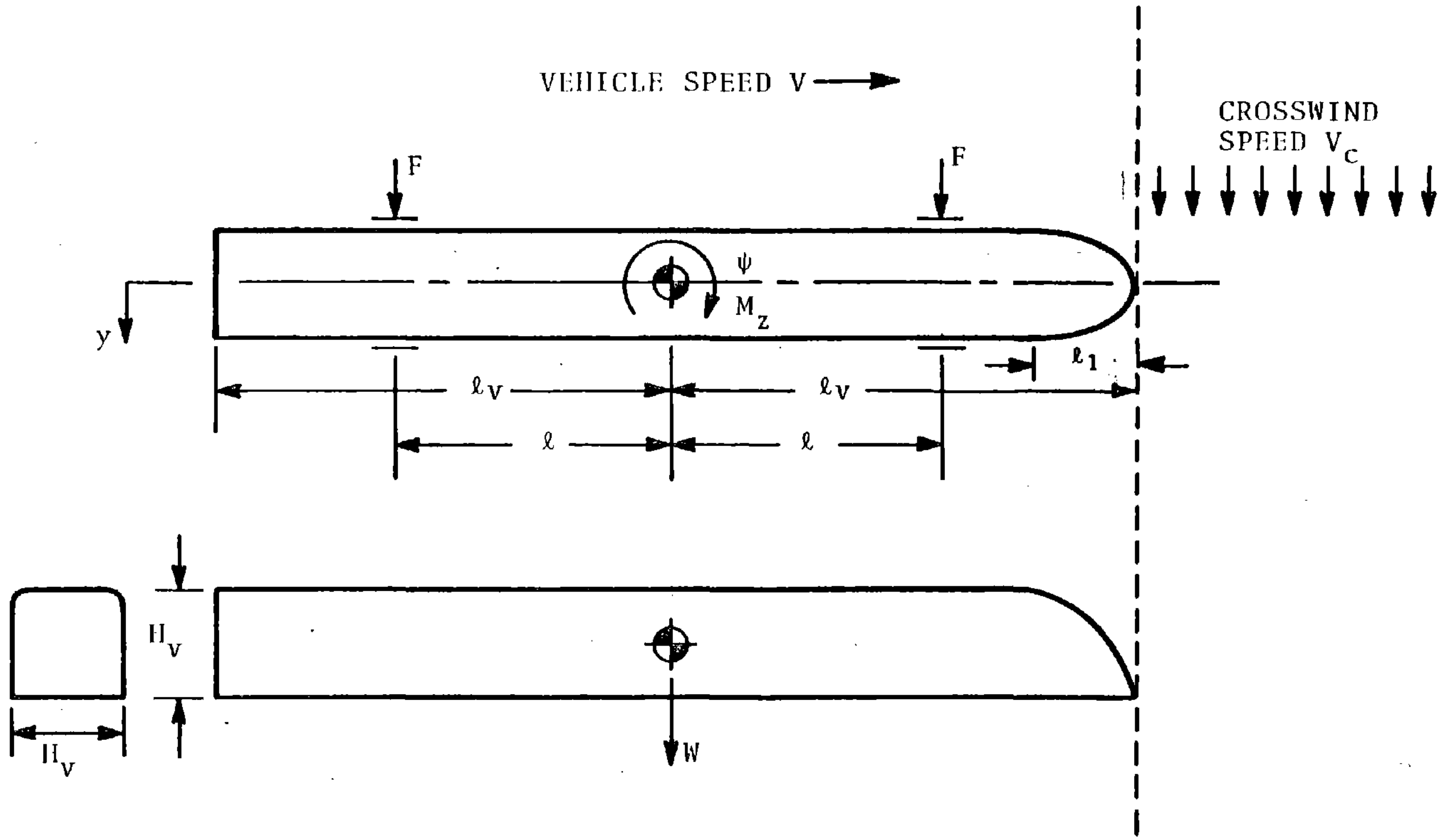

FIGURE 1-2. VEHICLE CONFIGURATION FOR ANALYSIS

concerned with the dynamic response of the vehicle to aerodynamic loads, the effect of guideway irregularities is neglected. It is assumed that motions due to such irregularities are small compared to the gust-induced motions.

In canonical form, the equations of motion in sway and yaw modes can be written as:

sway: $$(s^2 + 2\zeta_y\omega_y\ s + \omega_y^2)y = \frac{F_{aero}}{m_a} \tag{1}$$

yaw: $$(s^2 + 2\zeta_\psi\omega_\psi s + \omega_\psi^2)\psi = \frac{M_z}{I_a} \tag{2}$$

where,

m_a = vehicle apparent mass

ζ_y = damping ratio in sway mode

ω_y = natural frequency in sway mode

y = sway (lateral) displacement

F_{aero} = aerodynamic load in lateral direction

I_a = vehicle apparent moment of inertia

ζ_ψ = damping ratio in yaw mode

ω_ψ = natural frequency in yaw mode

ψ = yaw displacement

M_z = aerodynamic torque on the vehicle

s = Laplace operator

These equations can be expressed, using the state variable formulation, as a system of four first-order differential equations. Defining:

$$
\left.
\begin{aligned}
y_1 &= y \\
y_2 &= \dot{y} = \dot{y}_1 \\
y_3 &= \psi \\
\text{and } y_4 &= \dot{\psi} = \dot{y}_3
\end{aligned}
\right\} \qquad (3)
$$

the equations become

$$
\left.
\begin{aligned}
\dot{y}_1 &= y_2 \\
\dot{y}_2 &= \omega_y^2 \, y_1 - (2\zeta_y \omega_y) y_2 + \frac{F_{aero}}{m_a} \\
\dot{y}_3 &= y_4 \\
\dot{y}_4 &= \omega_\psi^2 y_3 - (2\zeta_\psi \omega_\psi) y_4 + \frac{M_z}{I_a}
\end{aligned}
\right\} \qquad (4)
$$

i.e.,

$$
\frac{d}{dt}
\begin{bmatrix} y_1 \\ y_2 \\ y_3 \\ y_4 \end{bmatrix}
=
\begin{bmatrix}
0 & 1 & 0 & 0 \\
-\omega_y^2 & -2\zeta_y \omega_y & 0 & 0 \\
0 & 0 & 0 & 1 \\
0 & 0 & -\omega_\psi^2 & -2\zeta_\psi \omega_\psi
\end{bmatrix}
\begin{bmatrix} y_1 \\ y_2 \\ y_3 \\ y_4 \end{bmatrix}
+
\begin{bmatrix} 0 \\ F_{aero}/m_a \\ 0 \\ M_z/I_a \end{bmatrix}
\qquad (5)
$$

The parameters ω_y and ζ_y can be selected on the basis of specific design considerations. Corresponding parameters ω_ψ and ζ_ψ can be obtained from the vehicle configuration as follows. Assuming,

2K = equivalent stiffness of magnetic suspension

2b = equivalent damping of magnetic suspension

m = vehicle mass

I = vehicle mass moment of inertia

F = lateral suspension force

observe that

$$\omega_y = \sqrt{\frac{2K}{m}} \tag{6}$$

$$\omega_\psi = \sqrt{\frac{K_\psi}{I}} \tag{7}$$

for a vehicle with uniformly distributed mass

$$I = \frac{1}{12} m (2\ell_v)^2 = \frac{1}{3} m\ell_v^2 \tag{8}$$

$$K_\psi = \frac{T}{\psi} = \frac{F(2\ell)}{(y/\ell)} = \left(\frac{2F}{y}\right) \ell^2$$

$$= 2K\ell^2 \tag{9}$$

Therefore,

$$\omega_\psi = \sqrt{\frac{K_\psi}{I}}$$

$$= \sqrt{\frac{2K\ell^2}{\frac{1}{3}m\ v^2}} = \sqrt{\frac{2K}{m}} \sqrt{3\left(\frac{\ell}{\ell_v}\right)^2}$$

$$= \omega_y \left(\frac{\ell}{\ell_v}\right)\sqrt{3}$$

$$= 1.732 \left(\frac{\ell}{\ell_v}\right) \omega_y \tag{10}$$

A similar relationship can be derived for the damping ratios ζ_ψ and ζ_y as shown below. Observe that

$$b_\psi = 2b\ell^2 \tag{11}$$

$$\zeta_y = \frac{1}{2} \quad \frac{(2b)}{\sqrt{m(2K)}} \tag{12}$$

and

$$\zeta_\psi = \frac{1}{2} \quad \frac{b_\psi}{\sqrt{IK_\psi}}$$

$$= \frac{1}{2} \cdot \frac{2b\ell^2}{\sqrt{\frac{1}{3} m\ell_v^2 \quad 2 \; K\ell^2}}$$

$$= \frac{1}{2} \cdot \frac{2b}{\sqrt{m(2K)}} \cdot \left(\frac{\ell}{\ell_v}\right) \sqrt{3}$$

$$= \zeta_y \left(\frac{\ell}{\ell_v}\right) \sqrt{3}$$

$$= 1.732 \left(\frac{\ell}{\ell_v}\right) \zeta_y \tag{13}$$

1.3 COMPUTATION OF MAGNET FORCES

The force exerted by the magnetic suspension can be computed by observing that the inertial force is the difference between the aerodynamic force, which is externally applied to the vehicle, and the restoring force exerted by the magnetic suspension. The magnetic suspension force has two components: one is contributed by sway, and the other by yaw. These two components can be calculated as follows:

$$m\ddot{y} = F_{aero} - F_{mag_{(s)}} \tag{14}$$

where $F_{mag_{(s)}}$ = magnetic suspension force in sway, and the other terms have been defined previously. Solving for $F_{mag_{(s)}}$ gives

$$\begin{aligned} F_{mag_{(s)}} &= F_{aero} - m\ddot{y} \\ &= m_a\ (s^2 + 2\zeta_y \omega_y s + \omega_y^2)\ y - ms^2 y \\ &= [(m_a - m)s^2 + m_a(2\ \zeta_y \omega_y)s + m_a \omega_y^2]\ y \end{aligned} \tag{15}$$

A similar relation may be developed for the yaw motions. The total force due to magnetic suspension is

$$F_{mag} = F_{mag_{(s)}} + F_{mag_{(y)}} \tag{16}$$

$$\begin{aligned} &= [(m_a - m)s^2 + m_a(2\zeta_y \omega_y)\ s + m_a \omega_y^2]\ y \\ &+ \frac{1}{2\ell}\ [(I_a - I)s^2 + I_a(2\ \zeta_\psi \omega_\psi)\ \ s + I_a \omega_\psi^2]\psi \end{aligned} \tag{17}$$

The guidance-to-lift ratio is given by the ratio of F_{mag} to the vehicle weight parameter. In the present analysis the apparent mass factor is defined as the ratio of m_a; the apparent mass of the vehicle, (the increase in actual mass of the vehicle resulting from the use of acceleration feedback in control), and the actual vehicle mass.

1.4 VEHICLE AERODYNAMIC FORCES AND MOMENTS

Aerodynamic gust loading can be important for operating speeds of magnetically levitated vehicle configurations presently under consideration. For example, protection against gust loads may become a critical factor in suspension design and control strategy selections. The aerodynamic loading depends upon vehicle profile and guideway contour, speed of wind, and the direction of flow.

Several procedures have appeard in the literature [28-33] for computation of aerodynamic loading due to wind gusts. The most important loads for suspension design consist of the side force and the yaw moments which are given by

$$F_{aero} = C_y S q \tag{18}$$

$$M_z = C_n S \ell_v q \tag{19}$$

where

S = reference area presented to the wind

q = dynamic pressure, which is a function of air density, and vehicle crosswind relative velocity

ℓ_v = length of the vehicle

C_y = Force coefficient

C_n = Moment coefficient

The aerodynamic loading is assumed to consist of two parts: one the non-viscous, slender body part; the other, the viscous, crossflow part [34]. The corresponding side force and yaw moment equations can be expressed as:

$$F_{aero} = qS(C_{y_{fs}} + C_{y_c}) \tag{20}$$

$$M_z = qS\ell_v(C_{n_{fs}} + C_{n_c}) \tag{21}$$

where

$C_{y_{fs}}$ = side force coefficient due to slender-body part

C_{y_c} = sideforce coefficient due to crossflow

$C_{n_{fs}}$ = yaw moment coefficient due to slender body part

C_{n_c} = yaw moment coefficient due to crossflow

the relative wind velocity is given by

$$V_r = [V^2 + V_c^2]^{1/2} \tag{22}$$

for a vehicle moving at a speed V entering a crosswind gust of velocity V_c. The wind impacts the vehicle at the side slip angle β given by

$$\beta = \tan^{-1} (V_c/V) \tag{23}$$

The reference area S presented to the wind is a function of the vehicle height H_V, and for the cross-sectional shape chosen in the present analysis is given by

$$S = (\pi/2)\ H_V^2 \tag{24}$$

The dynamic pressure q is given by

$$q = \frac{1}{2}\ \rho\ V_r^2 \tag{25}$$

for air density ρ and relative windspeed V_r.

For the slender-body force and moment coefficients, the following expressions are provided [34].

$$C_{y_{fs}} = \begin{cases} 2\beta x\ (2-x) & : x < 1 \\ 2\beta & : x \geq 1 \end{cases} \qquad \ldots \qquad (26)$$

and

$$C_{n_{fs}} = \frac{1}{2} \quad C_{y_{fs}}$$

$$- \begin{cases} 2\beta(\lambda_1/\lambda)x^2(1-2x/3) & : x < 1 \\ 2\beta(\lambda_1/\lambda)/3 & : x \geq 1 \end{cases} \qquad (27)$$

where

$x = Vt/\ell_1$ (28)

t = time after gust entry begins

ℓ_1 = length of nose section of the vehicle

$\lambda_1 = \ell_1/H_v$

$\lambda = \ell_v/H_v$

The viscous cross-flow part of (20) and (21) is due to the fact that flow separates off the side of the vehicle, producing contributions to the force and moment which become increasingly important at higher crosswind angles. The analytical method for computing these contributions follows the analysis by Bryson [35], who considered symmetric vortex separation on circular cylinders. This geometry applies directly to the case of a vehicle body of semicircular cross-section near the ground, as shown in Figure 1-3. In a coordinate system fixed to the fluid, the penetration of a cross-sectional plane by the body causes an unsteady motion. At early instants of time, corresponding to the front of the body, the vortices (i.e., the real vortex and the imaginary vortex) are located near the separation points and do not cause a large force. At later times, the vortices grow in strength and move downstream, thus causing an increasingly large suction force on the corresponding cross-section of the body. As these vortices pass further downstream, the force then decreases. Bryson's theory indicates the net force would go to zero, but a simple and useful modification is to assume the force never drops below the measured steady-state value for the drag on a circular cylinder. The result is the Modified-Bryson function $g(\sigma)$ shown in Figure 1-4. This function is used to predict forces and moments as prescribed in [34]*:

$$C_{yc} = \begin{cases} \left(\frac{2k\beta}{\pi}\right) \int_0^{\beta\lambda z} g(\sigma)\, d\sigma & : z < 1 \\ \left(\frac{2k\beta}{\pi}\right) \int_0^{\beta\lambda} g(\sigma)\, d\sigma & : z \geq 1 \end{cases} \tag{29}$$

*These equations for the stationary gust can be obtained from [30] by simply eliminating the unsteady terms due to immersion in the sudden gust field.

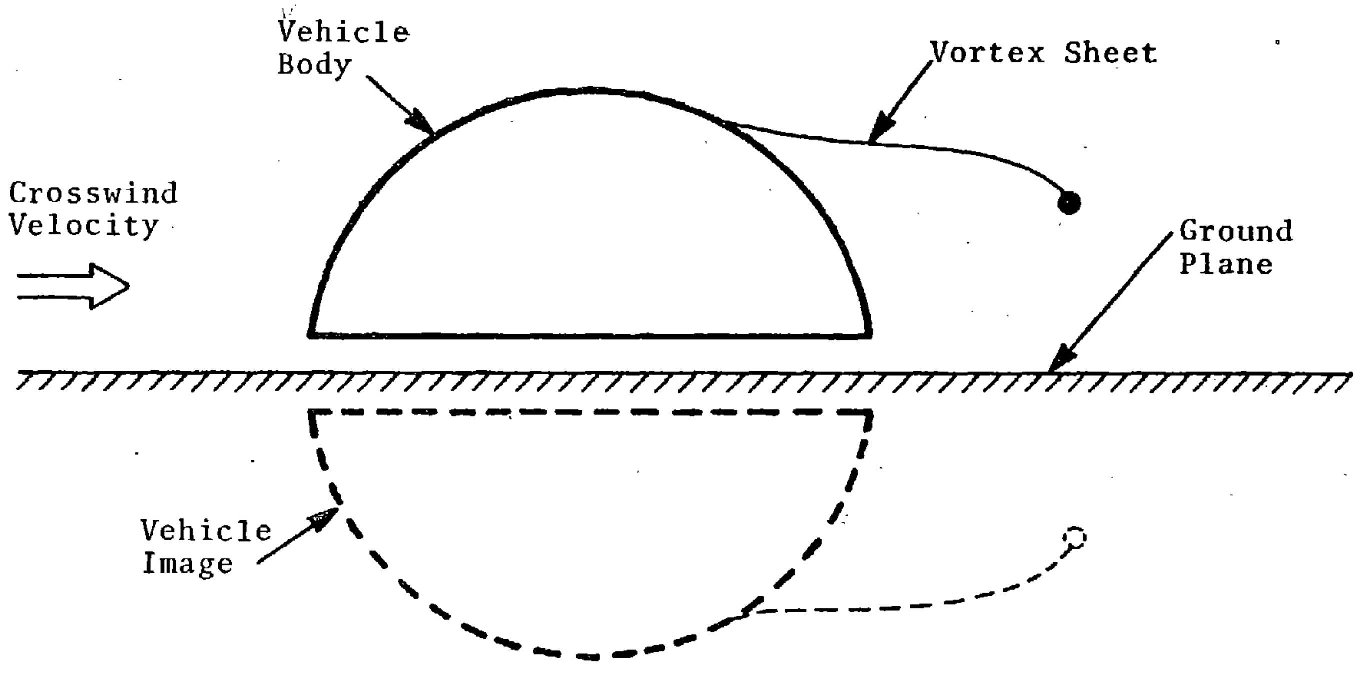

FIGURE 1-3. VORTEX SEPARATION OFF A VEHICLE OF SEMICIRCULAR CROSS-SECTION NEAR THE GROUND

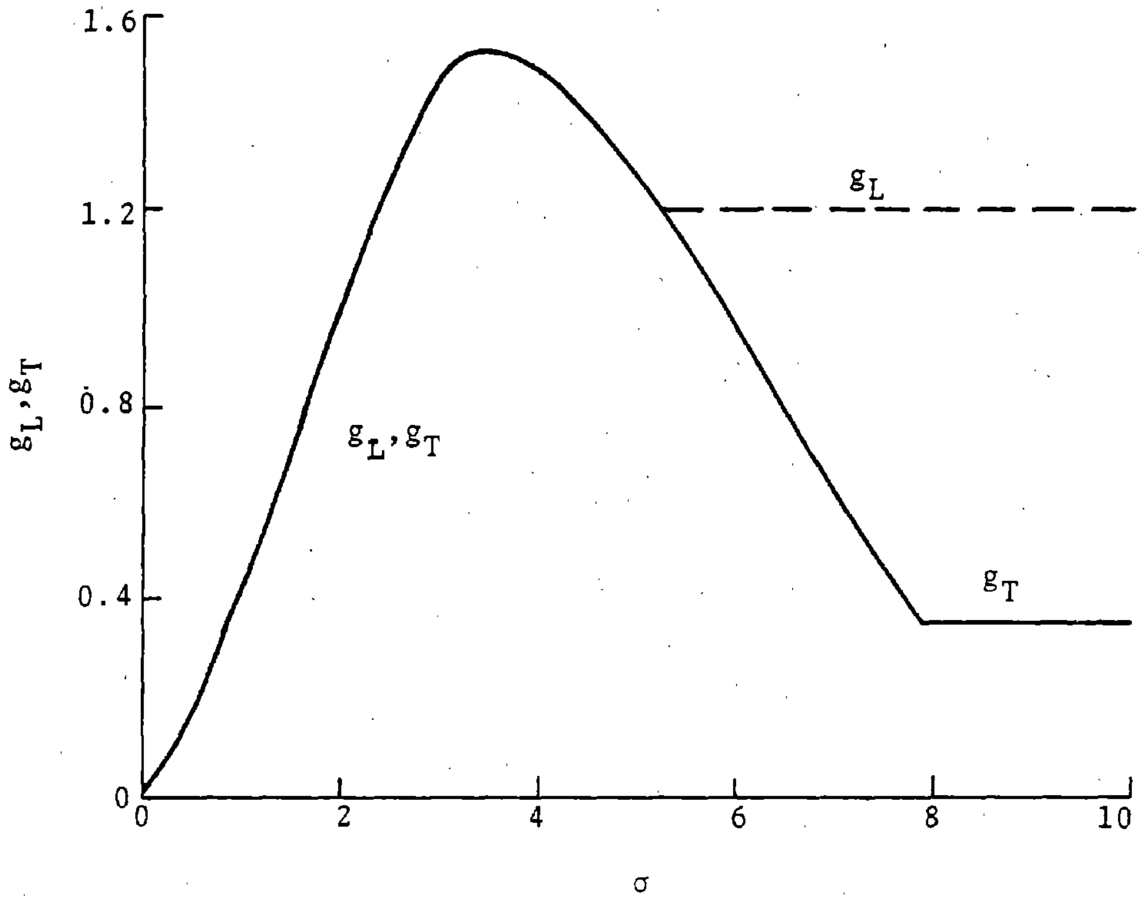

FIGURE 1-4. MODIFIED-BRYSON FUNCTION USED IN EQS. 29 AND 30

and

$$C_{nc} = \frac{1}{2} C_{y_c} \cdot \begin{cases} \left(\frac{2k}{\pi\lambda}\right) \displaystyle\int_0^{\beta\lambda z} \sigma g(\sigma) d\sigma & : z < 1 \\ \left(\frac{2k}{\pi\lambda}\right) \displaystyle\int_0^{\beta\lambda} \sigma g(\sigma) d\sigma & : z \geq 1 \end{cases} \quad (30)$$

where,

$$z = Vt/\ell_V \quad (31)$$

k = configuration factor (used as unity in the present analysis)

$g(\sigma)$ = modified-Bryson function plotted in Figure 1-4.

The configuration factor k was taken as unity because this value was found to give the best correlation with experimental data [31].

Figure 1-4 shows the modified Bryson function and has two curves, the dotted line portion corresponding to laminar, and the solid line portion corresponding to turbulent flow [30]. The selection of the appropriate curve is made based upon whether the boundary layer on the body is laminar or turbulent. In most instances the solid-line portion is used except for models in wind tunnels tested at subcritical crossflow Reynolds numbers. The configuration factor k incorporates the effects of body cross-section and nose profile.

Using the following vehicle parameters, aerodynamic force and moment computations were made for three vehicle speeds of 150, 240 and 300 mi/hr.

vehicle length	= 94.2 ft
nose length	= 15.3 ft
vehicle maximum height	= 10.7 ft
crosswind speed	= 60 mi/hr

The computed values of force and moment are given in Tables 1-1, 1-2 and 1-3 for the case of three vehicle speeds. Corresponding plots are shown in Figures 1-5 and 1-6.

It will be noted that the aerodynamic side force increases from zero to a final maximum value as the vehicle enters into the side gust field. The rate of increase depends upon vehicle velocity. Similarly, the yawing moment increases rapidly from zero to some large value, remains relatively constant for a short duration and then decreases to a final steady-state value. The higher the vehicle speed, the faster is the rise in yawing moment.

TABLE 1-1. AERODYNAMIC FORCES AND MOMENTS AT VEHICLE SPEED OF 150 MPH

t (SEC)	F_{aero} (LB)	M_z(FT-LB)
0.000	0.	0.
0.0200	3,800	24,776
0.0400	5,200	187,497
0.0600	6,900	387,700
0.0695	7,400	388,920
0.1000	7,800	394,832
0.2000	9,100	410,467
0.3000	11,200	392,996
0.4000	14,800	306,805
0.4288	16,500	265,202
0.5000	16,500	265,202
0.6000	16,500	265,202
0.7000	16,500	265,202
0.8000	16,500	265,202
0.9000	16,500	265,202
1.0000	16,500	265,202

TABLE 1-2. AERODYNAMIC FORCES AND MOMENTS AT VEHICLE SPEED OF 240 MPH

t	F_{aero}(LB.)	M_z(FT-LB)
0.0	0	0
0.01	5,617	2,59,846
0.02	9,785	4,45,298
0.04	13,796	6,40,196
0.10	14,438	6,29,574
0.15	15,252	6,31,631
0.20	16,392	6,14,153
0.25	17,857	5,67,023
0.2676	18,452	5,40,943
0.30	18,452	5,40,943
0.50	18,452	5,40,943
0.70	18,452	5,40,943
1.00	18,452	5,40,943

TABLE 1-3. AERODYNAMIC FORCES AND MOMENTS AT VEHICLE SPEED OF 300 MPH

t(SEC)	F_{aero}(LB)	M_z(FT-LB)
0	0	0
0.01	8,190	4,09,335
0.02	13,954	6,71,175
0.03	16,743	7,83,975
0.10	17,804	8,09,010
0.15	18,822	8,21,751
0.20	20,246	7,50,982
0.2141	20,722	7,27,800
0.30	20,722	7,27,800
0.50	20,722	7,27,800
0.70	20,722	7,27,800
1.00	20,722	7,27,800

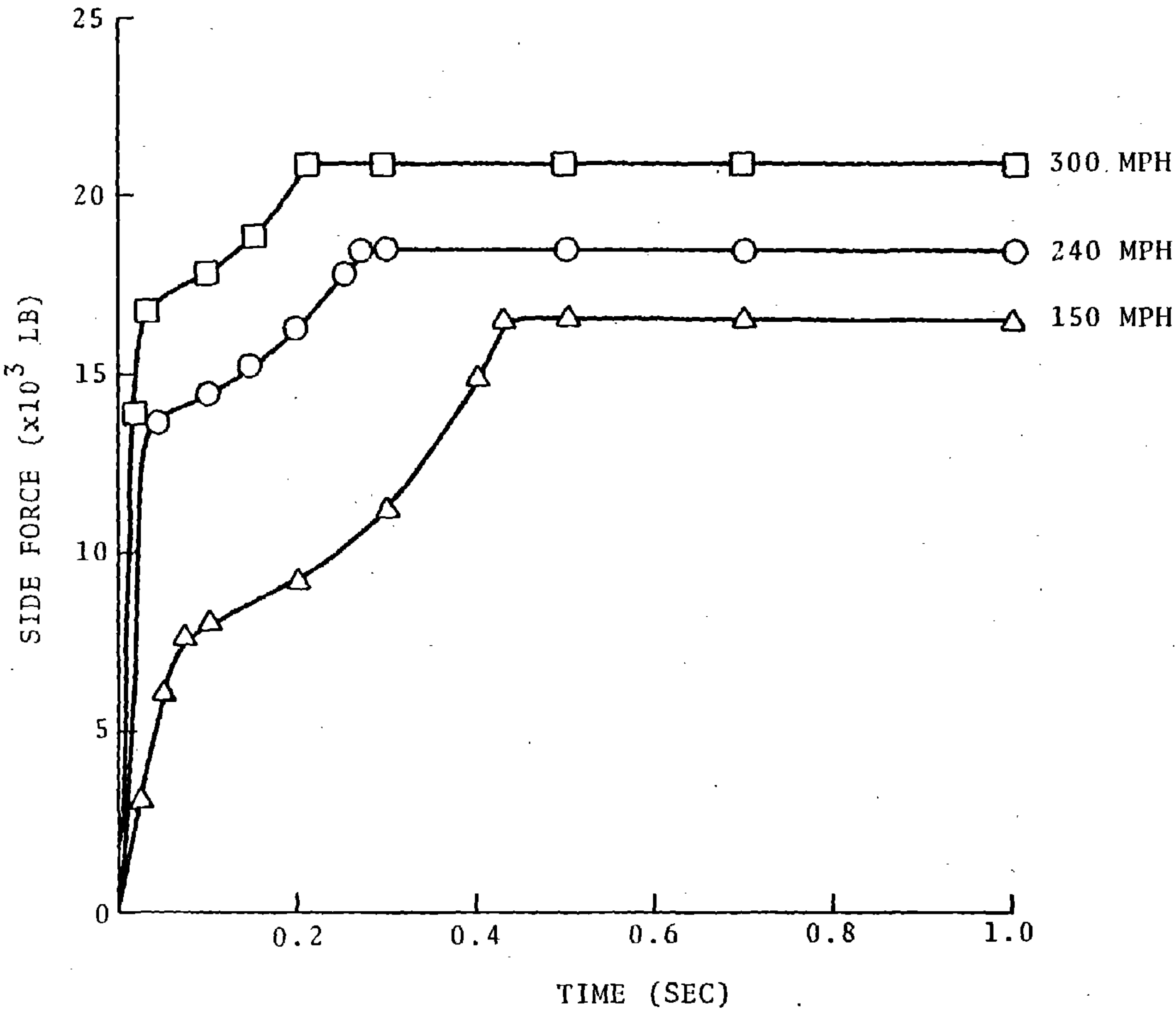

FIGURE 1-5. SIDE FORCE (LB) AT DIFFERENT VEHICLE SPEEDS

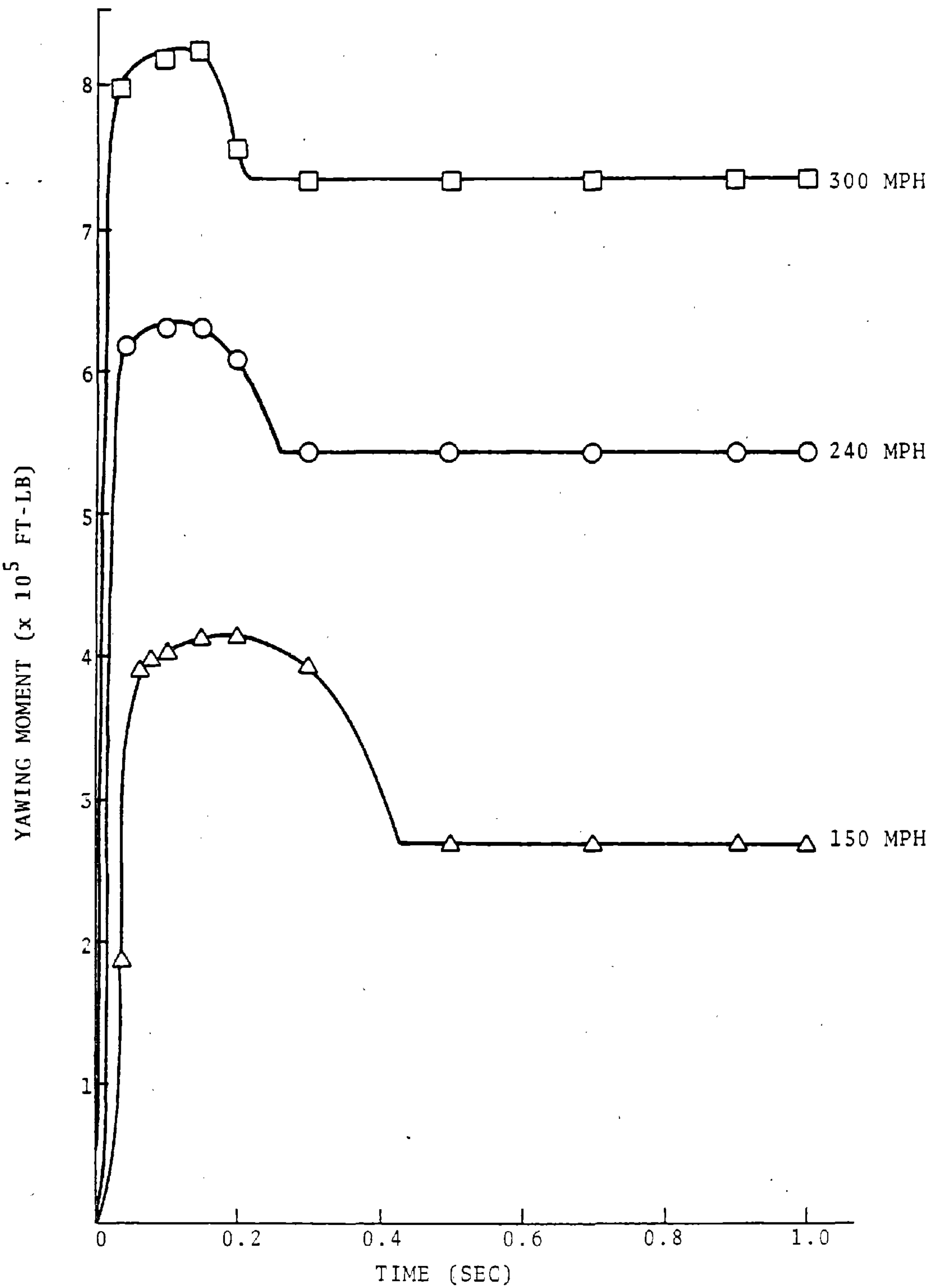

FIGURE 1-6. YAWING MOMENT (FT-LB) AT VARIOUS SPEEDS

2. FORCE AND MOMENT APPROXIMATION

For the purposes of dynamic simulation, the force and moment temporal plots were represented by four-segment piecewise linear approximations. Figure 2-1 shows such approximations for a vehicle speed of 150 mi/hr. Using this technique, linear relationships can be derived to express analytically the time dependence of side force and yawing moment. Values shown in parentheses in Figure 2-1 represent break-point values. For the case illustrated (i.e., 150 mi/hr) the following relationships are obtained:

<u>(A) SIDE FORCE</u>

<u>Segment 1</u>: $0 \leq t \leq 0.06$

slope $k_1 = (7.6 \times 10^3)/0.06 = 126{,}666$

$F_{aero} = k_1 t$

<u>Segment 2:</u> $0.06 \leq t \leq 0.3$

slope $k_2 = (11.0-7.6) \times 10^3/(0.3-0.06)$

$= 14{,}167$

$F_{aero} = k_2(t-0.06) + 7{,}600$

<u>Segment 3</u>: $0.4286 \leq t \leq 0.3$

slope $k_3 = (16.5-11) \times 10^3/(0.428-0.3)$

$= 5.5 \times 10^3/0.128$

$= 42{,}969$

$F_{aero} = k_3(t-0.3) + 11{,}000$

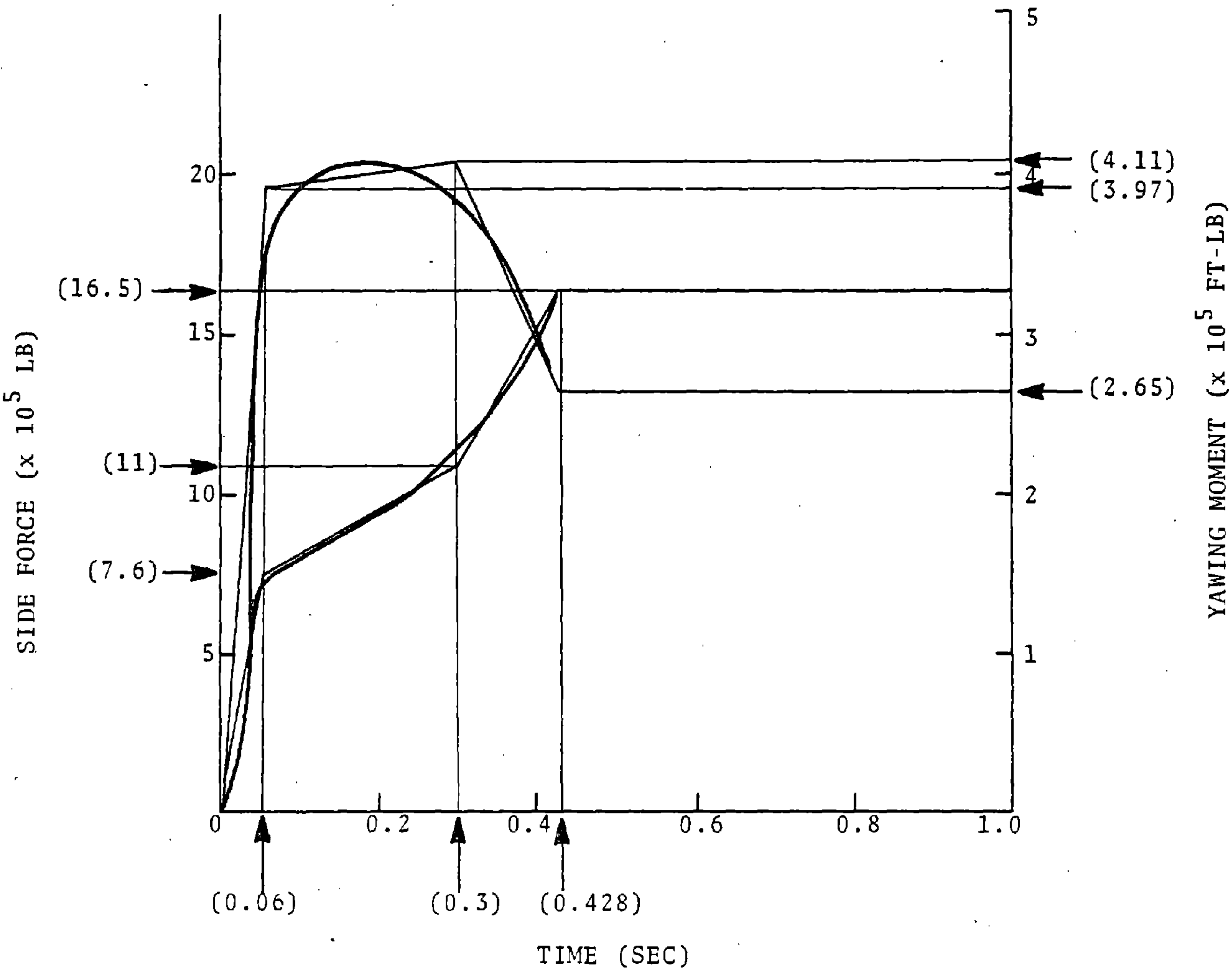

FIGURE 2-1. SIDE FORCE AND YAWING MOMENT APPROXIMATION BY PIECEWISE LINEAR SEGMENTS

Segment 4: $t \geq 0.428$

$$F_{aero} = 16{,}500 \text{ lb.}$$

Similarly, four-segment straight line representations can be obtained for the yawing moment curve.

(B) - YAWING MOMENT

Segment 1: $0 \leq t \leq 0.06$

$$\text{slope } k_1 = (3.97 \times 10^5)/0.06$$
$$= 66.167 \times 10^5$$
$$M_z = k_1 t$$

Segment 2: $0.06 \leq t \leq 0.3$

$$\text{slope } k_2 = (4.11-3.97) \times 10^5/(0.3-0.06)$$
$$= 0.14 \times 10^5/0.24$$
$$= 0.58333 \times 10^5$$
$$M_z = k_2(t-0.06) + 3.97 \times 10^5$$

Segment 3: $0.30 \leq t \leq 0.428$

$$\text{slope } k_3 = (2.65-4.11) \times 10^5/(0.428-0.3)$$
$$= -1.46 \times 10^5/0.128$$
$$= -11.406 \times 10^5$$
$$M_z = k_3(t-0.3) + 4.11 \times 10^5$$

Segement 4: $t \geq 0.428$

$$M_z = 2.65 \times 10^5$$

2.1 DYNAMIC SIMULATION

The differential equations representing the dynamics of the magnetically suspended vehicle system were simulated on the DEC-20 digital computer available at the TSC Computation Center. Subprogram DYSYS (DYnamic SYstem Simulation) [36], originally developed at M.I.T., was modified for application to the system under consideration. The program is designed to solve a system of first-order differential equations using a fourth-order Runge-Kutta integration algorithm. The equations are included in subroutine EQSIM (EQuation SIMulator) which is called four times for each integration time step.

The following quantities were calculated using the computer program:

(1) lateral displacement and velocity

(2) yaw displacement and velocity

(3) total displacement at front of the vehicle

(4) total acceleration at front of the vehicle

(5) guidance-to-lift ratio.

2.2 RESULTS AND DISCUSSION

Digital computer simulations were run for the vehicle-suspension system using the following parametric values:

vehicle weight	65,000 lb
vehicle length	94.2 ft
location of magnetic suspension from ends	4.71 ft
length of nose section	15.30 ft
maximum height	10.70 ft

lateral natural frequency	1.50 Hz
lateral damping ratio	0.707
wind gust velocity	60 mi/hr

For each of vehicle speed values set at 150, 240, and 300 mi/hr, computational runs were made for apparent mass factors of 1, 2, and 3. The mass factor reflects the effect of acceleration feedback used in the control scheme for the magnetic suspension. An increase in speed of the vehicle, for a fixed wind gust velocity, leads to a decrease in side slip angle β.

Table 2-1 shows the summary of principal results obtained on the basis of the present analysis. Output information on transient response is plotted for vehicle speeds of 150, 240, and 300 mi/hr in Figures 2-2, 2-3, and 2-4, respectively. Each of the figures is shown for a different apparent mass factor to emphasize the behavior of various variables. At different mass factors it will be noted that similarity exists in various corresponding plots.

Displacement is computed near the front end of vehicle at the location of the magnetic suspension. This displacement is a combination of lateral and yaw effects. It increases rapidly as the vehicle enters the gust field, and eventually attains a steady-state value after few minor oscillations.

Acceleration is also computed near the vehicle front end at the location of magnetic suspension. It represents the effects of both lateral and yaw accelerations. As will be

TABLE 2-1. SUMMARY OF RESULTS
(PEAK VALUES OF VARIABLES)

VEHICLE SPEED (MPH)	SIDE SLIP ANGLE β (DEG)	MASS FACTOR	MAXIMUM DISPLACEMENT FT	MAXIMUM ACCELERATION FT/SEC^2	GUIDANCE-TO-LIFT RATIO
150	21.80	1	0.1291 (1.549")	6.849 (0.2127g)	0.3224
		2	0.06456(0.7741")	3.424 (0.10633g)	0.3122
		3	0.04304(0.5165")	2.283 (0.071g)	0.3087
240	14.036	1	0.1770 (2.214")	16.560 (0.514g)	0.4239
		2	0.0885 (1.062")	8.278 (0.257g)	0.4030
		3	0.0590(0.708")	5.518 (0.1713g)	0.3960
300	11.31	1	0.2148(2.577")	19.22 (0.5969g)	0.5105
		2	0.1074(1.288")	9.61 (0.2984g)	0.4807
		3	0.0716(0.8592")	6.407 (0.1989g)	0.4707

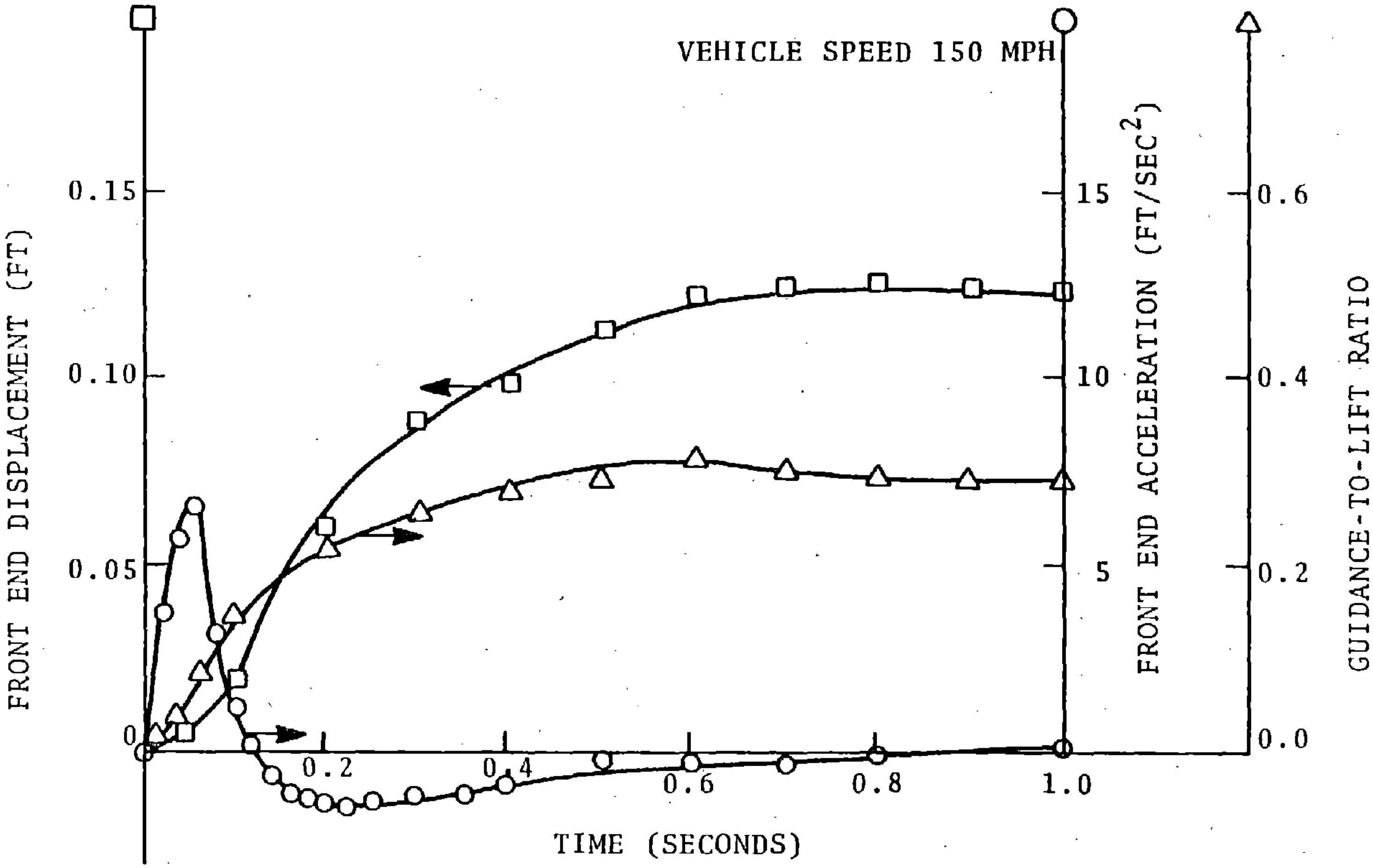

FIGURE 2-2. DISPLACEMENT, ACCELERATION, & GUIDANCE-TO-LIFT RATIO FOR APPARENT MASS FACTOR = 1

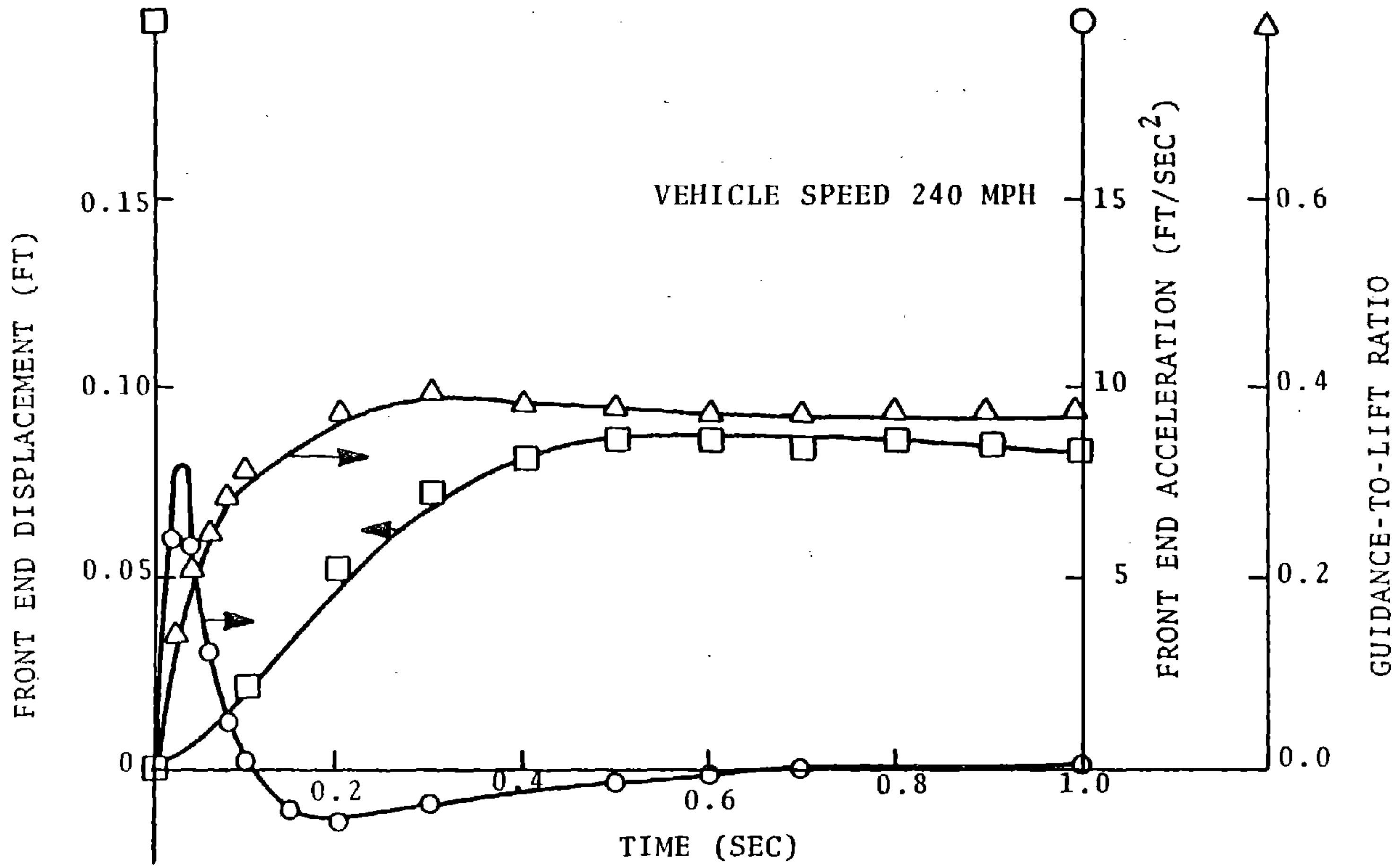

FIGURE 2-3. DISPLACEMENT, ACCELERATION & GUIDANCE-TO-LIFT RATIO FOR APPARENT MASS FACTOR = 2

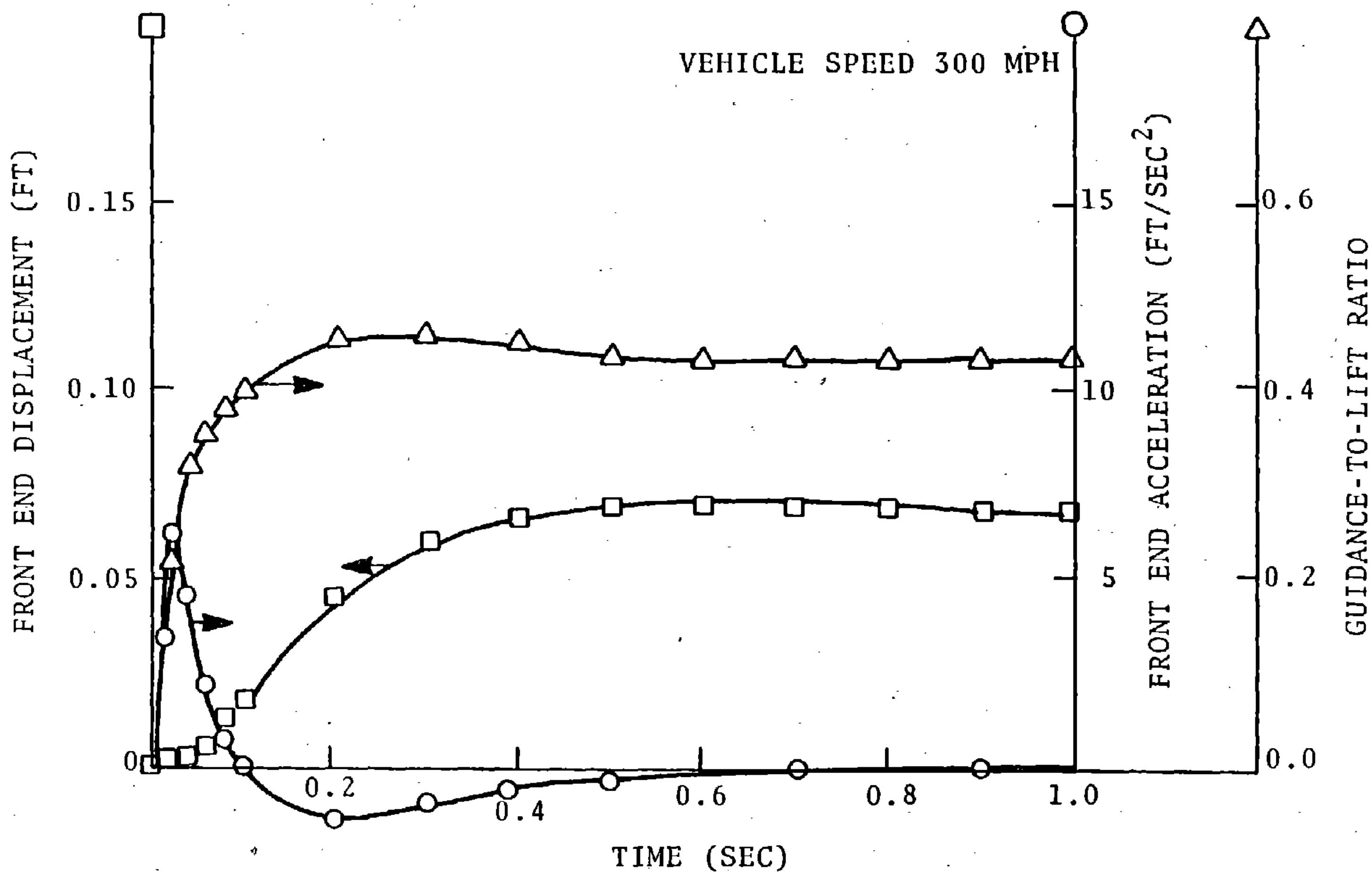

FIGURE 2-4. DISPLACEMENT, ACCELERATION, & GUIDANCE-TO-LIFT RATIO FOR APPARENT MASS FACTOR = 3

noted from the figures, it rises rapidly, approaching a sharp peak and then decreases rapidly to a negative value. Eventually, the acceleration reaches a zero value at steady-state conditions.

The guidance to lift ratio is obtained by evaluating the lateral force exerted by magnetic suspension and dividing it by the vehicle weight. A relatively small guidance force is required initially as the vehicle enters the gust field; however, as time progresses, higher and higher values of guidance forces are required until a peak asymptotic value is reached. The guidance-to-lift ratio is maintained essentially at this constant value until a steady-state condition is reached.

Figures 2-5, 2-6, and 2-7 represent the temporal description of displacement and acceleration variables at vehicle front end, and guidance-to-lift ratio for various apparent mass factors. For these simulations vehicle speed was maintained constant at 240 mi/hr. All curves show a similar trend for different apparent mass factors. Also, the steady-state value of displacements decreases with an increase in apparent mass factor, becoming approximately one-third for an apparent mass factor of 3 and one-half for the apparent mass factor of 2 as compared to the steady-state value corresponding to the apparent mass factor of unity. Similar behavior is observed for the peak values of acceleration. However, the steady-state values of acceleration for all

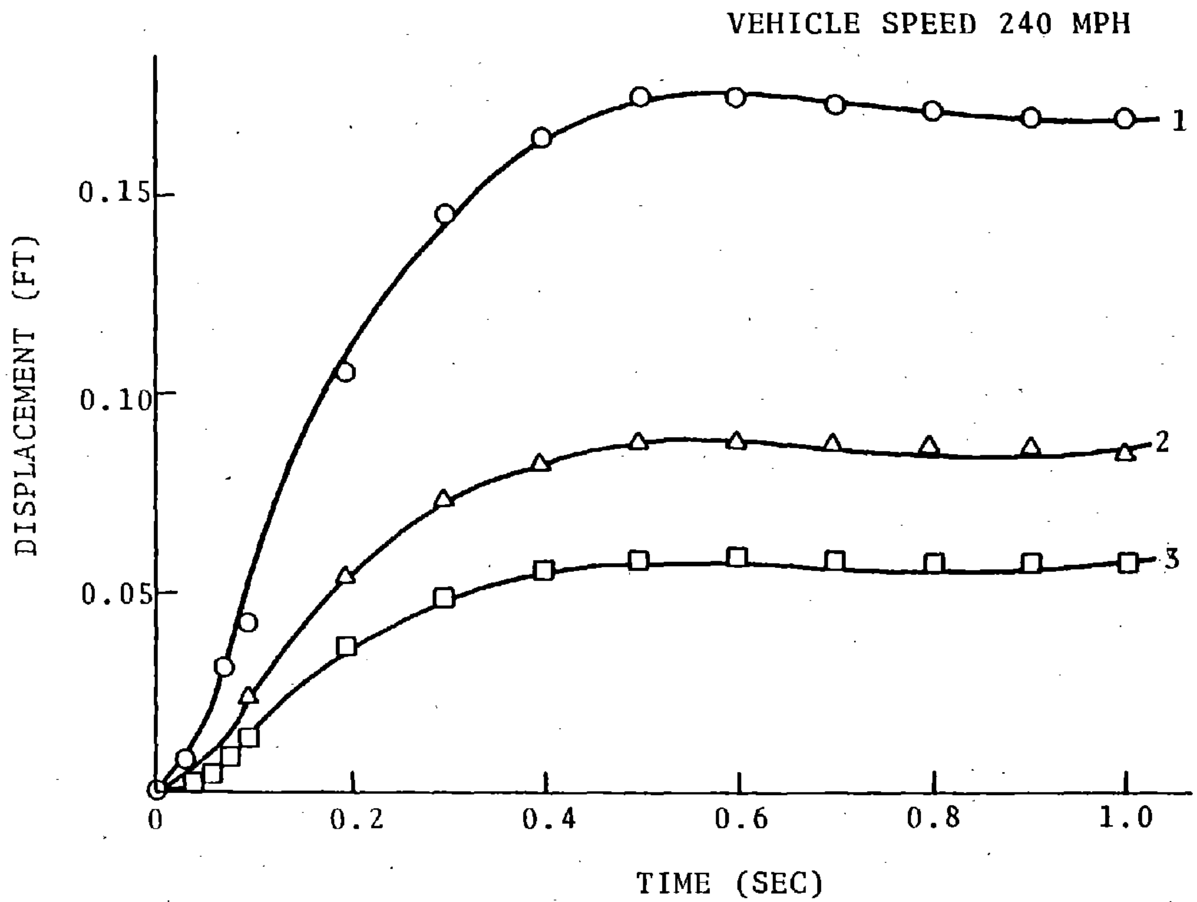

FIGURE 2-5. DISPLACEMENT AT FRONT OF VEHICLE (FT) AT VARIOUS APPARENT MASS FACTORS

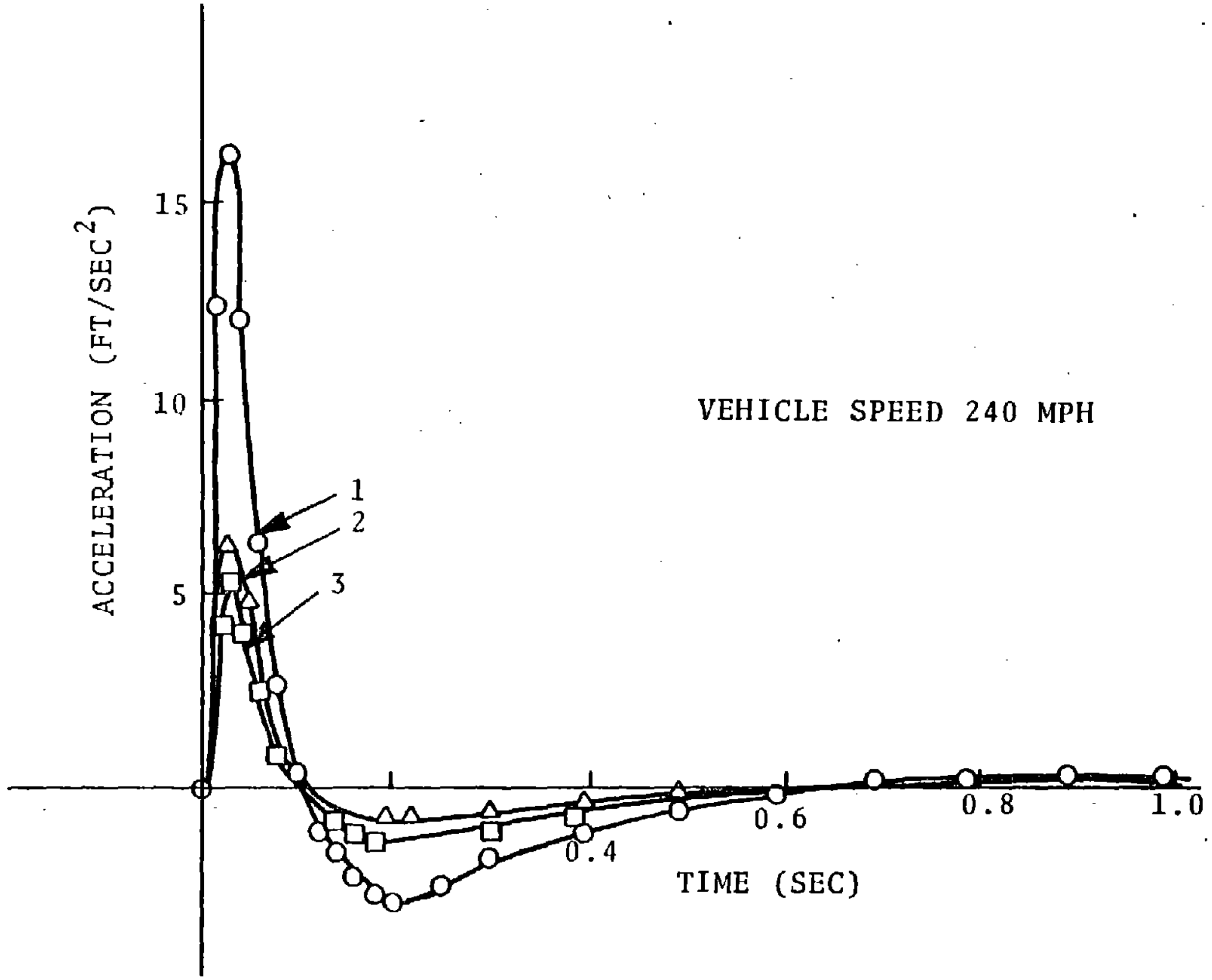

FIGURE 2-6. FRONT END ACCELERATION (FT /SEC^2) VS. TIME FOR VARIOUS APPARENT MASS FACTORS

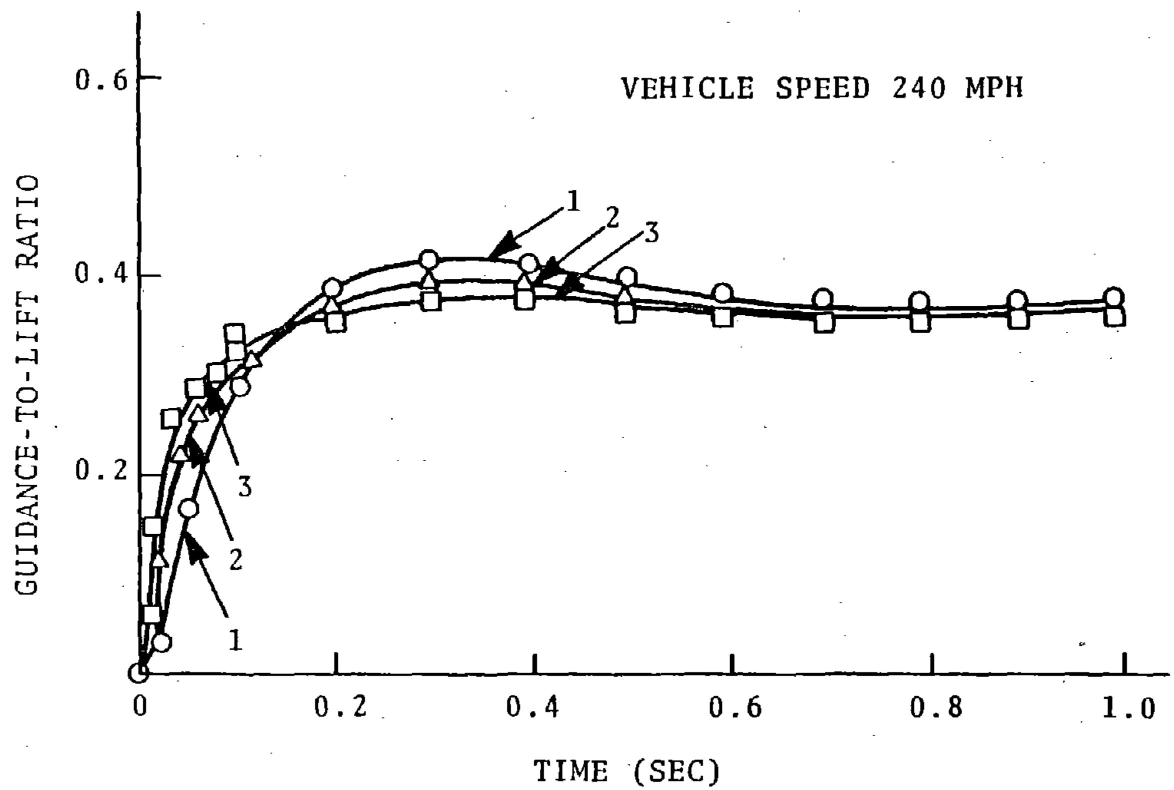

FIGURE 2-7. GUIDANCE-TO-LIFT RATIO FOR VARIOUS APPARENT MASS FACTORS

values of apparent mass factors is zero. The variation of guidance-to-lift ratio with time is similar to the 3 apparent mass factors considered. The three curves closely follow one another.

Figure 2-8 shows the vehicle peak lateral excursions at the location of magnetic suspension near the front end. These excursions increase with an increase in vehicle speed, although their values decrease as the apparent mass factor increases. Thus an increase in apparent mass factor has a positive influence toward improving the ride quality. Figure 2-9 presents the same information on peak vehicle displacement in parameter space.

Figure 2-10 shows the variation of peak acceleration at the front end of the vehicle with a change in vehicle speed. As in the case of displacement, the value of peak acceleration increases with an increase in vehicle speed. Also, an increase in apparent mass factor causes a decrease in peak acceleration. For example, at vehicle speed of 300 mi/hr, for apparent mass factor of 3 the peak acceleration is reduced to 33% of the peak acceleration when the apparent mass factor is one, and for apparent mass factor of 2, the corresponding value is reduced to 50%. Thus an increase in apparent mass factor again shows an improvement in ride quality by causing a reduction in peak acceleration levels.

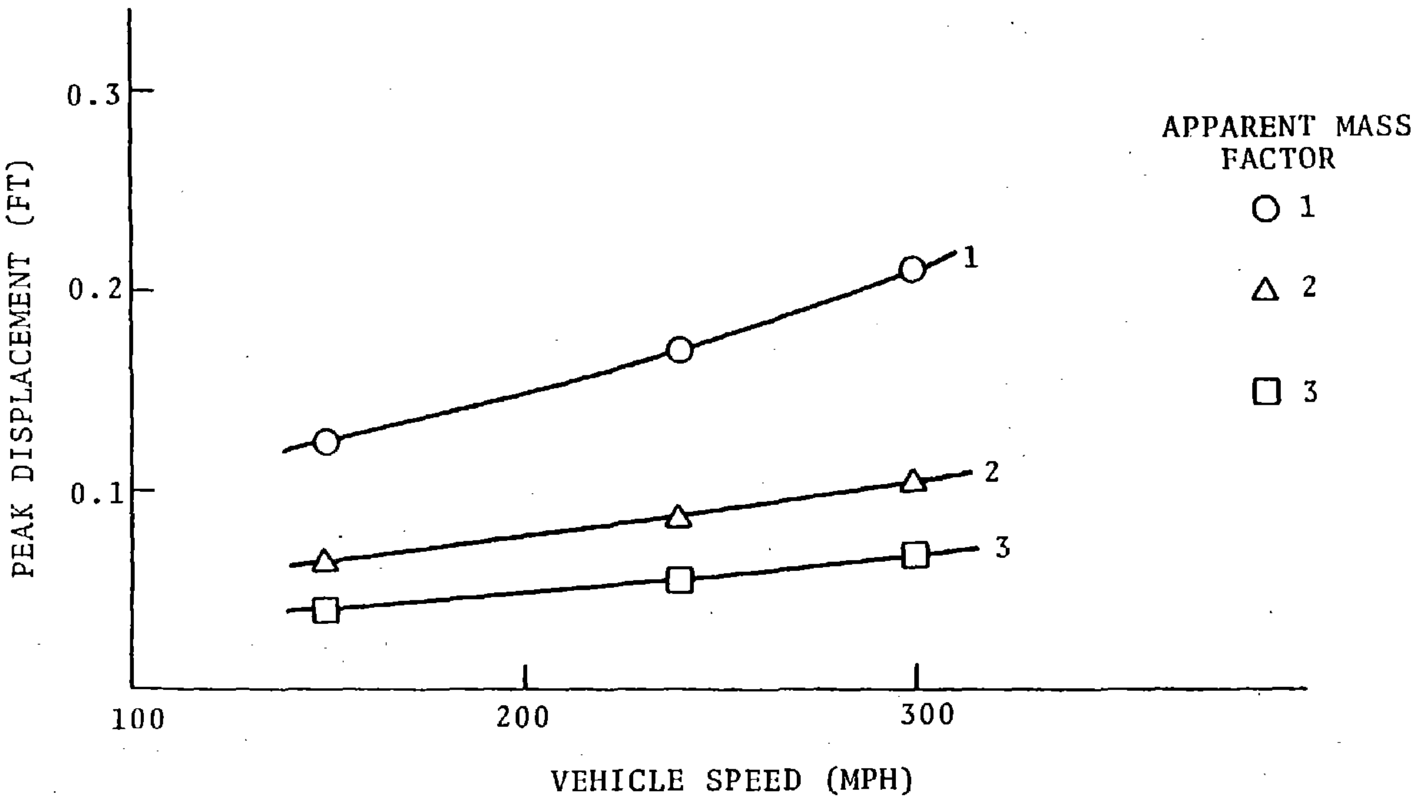

FIGURE 2-8. PEAK DISPLACEMENT VS. VEHICLE SPEED FOR VARIOUS APPARENT MASS FACTORS

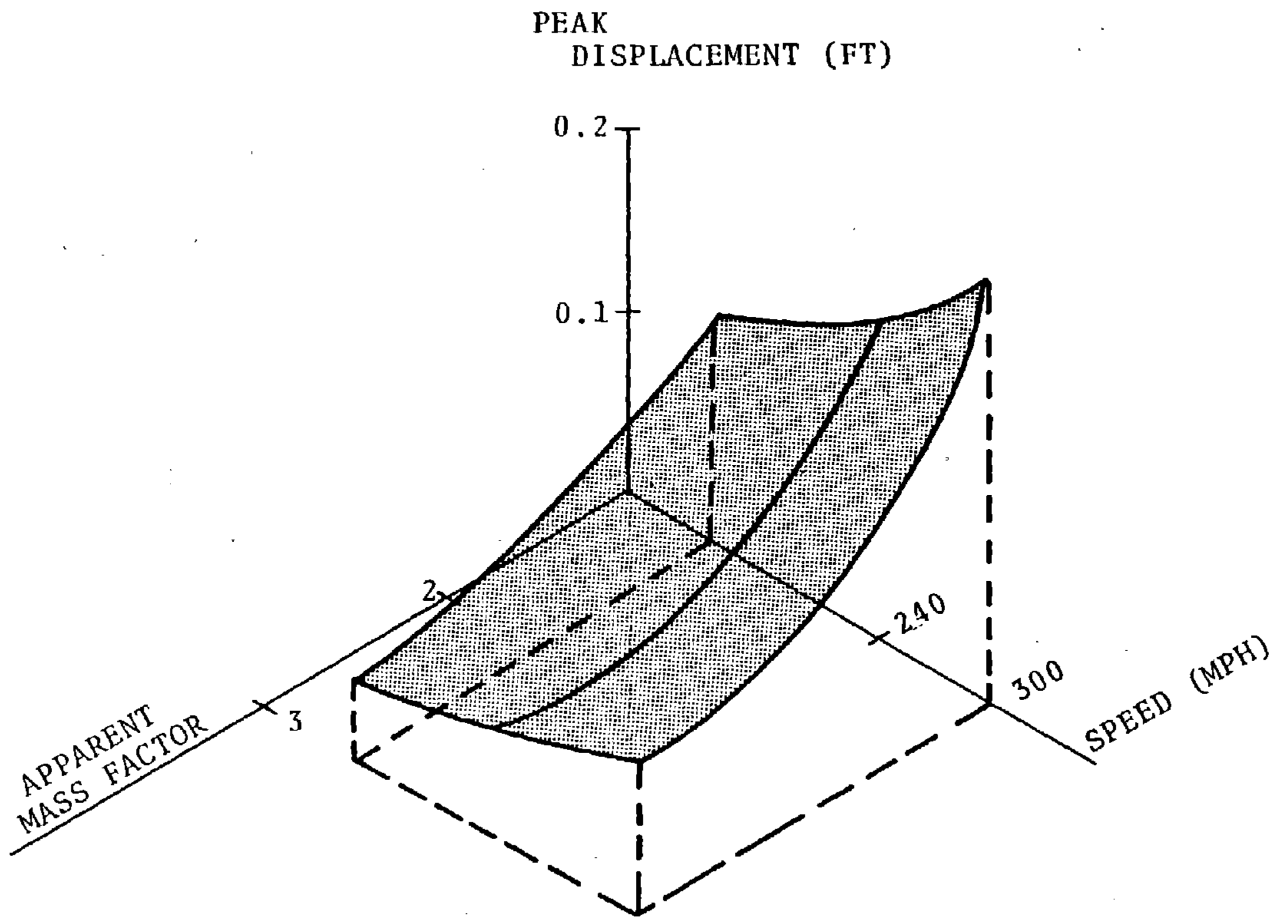

FIGURE 2-9. PARAMETER SPACE REPRESENTATION OF PEAK FRONT END DISPLACEMENT

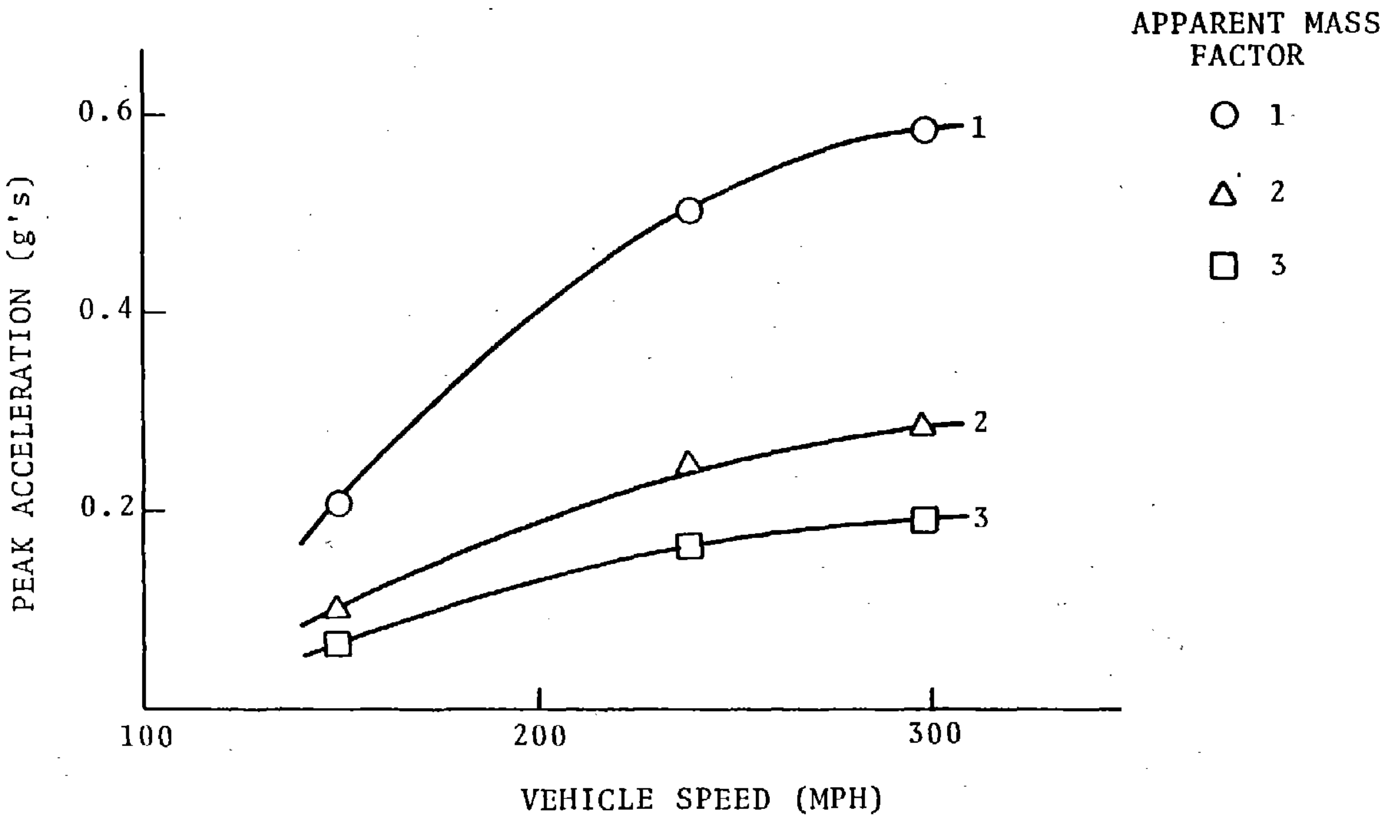

FIGURE 2-10. PEAK ACCELERATION (TRANSIENT) VS. VEHICLE SPEED

Finally, Figure 2-11 shows the change in peak values of guidance-to-lift ratios with a change in vehicle speed. As in the other two cases, the peak values increase with an increase in vehicle speed. Although the peak guidance-to-lift ratio decreases with an increase in apparent mass factor, when the vehicle speed is maintained constant, the change in peak values is not as significant as in the case of displacement or acceleration.

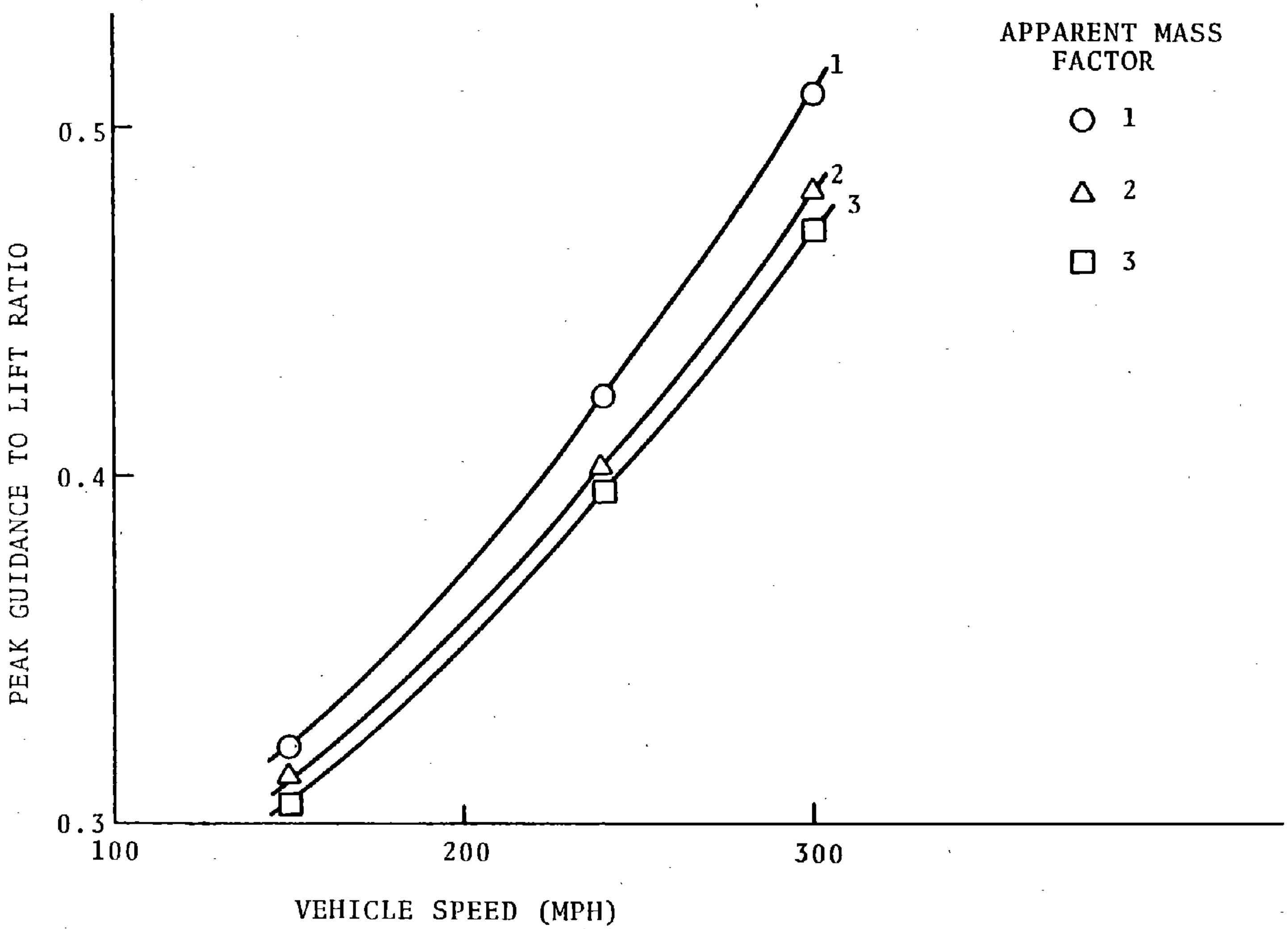

FIGURE 2-11. PEAK GUIDANCE-TO-LIFT RATIO VS. VEHICLE SPEED

3. CONCLUSIONS

In this report a two-degree-of-freedom dynamic model for a magnetically levitated finite length vehicle has been presented. The model has been parametrically evaluated for various speeds ranging from 150 to 300 mi/hr, for crosswind gusts at 60 mi/hr. For the chosen set of vehicle parameters, aerodynamic force and moment were computed at various vehicle speeds. Piecewise linear approximation of force and moment curves were obtained. Digital computer simulations were run to compute peak displacement and acceleration levels at the vehicle front end, and guidance-to-lift ratio for 3 apparent mass ratios.

The following conclusions can be reached on the basis of analysis presented in this report:

1. Apparent mass factor is an important parameter in that it can reduce the lateral excursions and peak vehicle displacements in a significant manner. Higher apparent mass factors lead to lower peak accelerations and displacements.

2. Forces and moments arising from aerodynamic gusts can present excessive loads on the vehicle and must be taken into account while designing vehicle suspension systems.

3. Yaw motions can contribute to excessive total lateral displacement and accelerations, and should be considered in any analysis and design.

RECOMMENDATIONS

The present analysis assumed the magnetic suspensions to be located close to the vehicle ends. The effect of several suspension blocks located uniformly along the length of the vehicle should be considered. Lateral guidance-to-lift ratio should be computed for such a configuration.

It has been shown in the present analysis that an increase in apparent mass of the vehicle has a beneficial effect in that the displacements and acceleration values are reduced at operating speeds. This should be further investigated and the limiting value of apparent mass from both practical and operational viewpoints should be established.

4. REFERENCES

1. Thornton, R. D., "Magnetic Levitation and Propulsion," IEEE Transaction on Magnetics, Vol. MAG-11, No. 4, July 1975.
2. Ward, J. D., "The Future Roles for Tracked Levitated Vehicle Systems," Transactions of the ASME, Journal of Dynamic Systems, Measurement and Control, Series G, Vol. 96, No. 2, June 1974.
3. Barrows, T. M., "Suspension Concepts for High-Speed Ground Transportation," Technology Review, Vol. 77, No. 8, July/August 1975.
4. Limbert, D. A., Weinberg, M. S., Wormley, D. N., and Richardson H. H., "Dynamic Performance and Control of Attractive Electromagnetic Tracked Levitated Vehicle Suspension Systems," Report No. EPL-75-72965-1, Department of Mechanical Engineering, M.I.T., Cambridge, MA, March 1975.
5. Sweet, L. M., "Analysis, Testing and Design of Plenum Air Cushion Suspensions, including Feeding System Dynamics," Ph.D. Thesis, Department of Mechanical Engineering, M.I.T., Caambridge, MA, August 1976.
6. Gutberlet, H. G., "The German Magnetic Transportation Program," IEEE Transactions on Magnetics, Vol. MAG-10, No. 3, September 1974.

7. Yamamura, S., "Magnetic Levitation Technology: Present Status and Prospects," IEEE Transactions on Magnetics, Vol. MAG-12, No. 6, November 1976.

8. Eggleton, P. L. and Rudback, N. E., "Status of Magnetic Levitation and Linear Motor Research Activities in Canada-1978, Paper Presented at the 11th Annual Japan-USA Transportation Research Panel, Washington, DC, January 22, 1979.

9. Gottzein, E. and Lange, B., "Magnetic Suspension Control Systems for the German High Speed Train," Second Inter-Society Conference on Transportation, Denver, CO, September 1975.

10. Hayashi, A., "An Alternative Plan to International Airport Access," Second Tokyo Transport Environmental Conference, Tokyo, Japan, 1977.

11. Yamamura, S. and Ito, T., "Analysis of Speed Characteristics of Attracting Magnet for Magnetic Levitation of Vehicles," IEEE Transactions on Magnetics, Vol. MAG-11, No. 5, September 1975.

12. Katz, R. M. et al., "Performance of Magnetic Suspensions for High Speed Vehicles Operating Over Flexible Guideways," Journal of Dynamic Systems, Measurement, and Control, Transactions of the ASME, Series G, Vol. 96, No. 2, June 1974.

13. Gottzein, et al., "Optimal Control of a Maglev Vehicle," Proceedings of the IUTAM Symposium, The Dynamics of Vehicles on Roads and Railway Tracks, H. E. Pacejka, (Ed.), Delft, The Netherlands, August 1975.

14. Katz, R. M., "The Investigation of the Dynamics of a Maglev Vehicle Traversing a Flexible Guideway: Theory and Experiment," Report No. MITRE MTR-7771, the Mitre Corporation, Metrek Division, McLean, VA. Prepared for the Office of Secretary, U.S. DOT, Washington, DC, June, 1978.

15. Borcherts, R. H. et al., "Parameter Optimization Studies of Magnetic Suspensions for High-Speed Ground Transportation," NTIS Clearinghouse, FRA-ORD&D-74-42, April 1974.

16. Meisenholder, S. G., and Wang, T.C., "Dynamic Analysis of an Electromagnetic Suspension System for a Suspended Vehicle System," TRW Systems Group, NTIS Clearinghouse, FRA-RT-71-1 (PB-211-592), January 1972.

17. Hayes, W. F., "High Speed Electrodynamic Maglev Guided Ground Transportation System Conceptual Design Study," Report No. LTR-CS-176, National Research Council, Ottawa, Canada, September 1977.

18. Status Seminar VI Reports on Tracked Long-Distance Traffic Magnetic Railway Development, Federal Ministry for Research and Technology, Technological Research and Development (Transport and Traffic), Constance, Germany, 1977.

19. Whe, H. et al., "Magnetically Suspended Vehicle with an Active Guideway, Presented at the 2nd International Hovering Craft Hydrofoil, and Advanced Systems Conference, Amsterdam, May 1976.

20. Coffee, H. T. et al., "The Feasibility of Magnetically Levitating High Speed Ground Vehicles," Stanford Research Institute, NTIS Clearinghouse, FRA-RT-72-39, February 1972.

21. Davis, L. C. et al., "Technical Feasibility of Magnetic Levitation as a Suspension System for High Speed Ground Transportation Vehicles," Ford Motor Co., NTIS Clearinghouse, FRA-RT-72-40, February 1972.

22. Wormley, D. N. et al., "Noncontacting Suspension and Propulsion for Ground Transportation," Final Second Year Report. Prepared for Office of University Research, U.S. DOT, Washington, DC, January 1979.

23. Reitz, J. R., "Preliminary Design Studies of Magnetic Suspensions for High Speed Ground Transportation," Ford Motor Company, Transportation Research and Planning Office, Report No. FRA-RT-73-27, NTIS Clearinghouse, (PB 223237). Prepared for Federal Railroad Administration, Office of Research, Development, and Demonstration, Washington, DC, March 1973.

24. Hammitt, A. G., "Aerodynamic Forces on Freight Trains, Vol I: "Wind Tunnel Tests of Containers," Andrew G. Hammitt Associates, Rancho Palos Verdes, CA, Report No. FRA/ORD-76-295.I, Prepared for FRA/USDOT, Office of R&D, Washington, DC, December 1976.

25. Grunwald, K. J., "Aerodynamic Characteristics of Vehicle Bodies at Crosswind Conditions in Ground Proximity," NASA Technical Note No. D-5935, NASA Langley Research Center, Hampton, VA, August 1970.

26. Wormley, D. N., et al., "Noncontacting Suspension and Propulsion for Ground Transportation," Final First Year Report. Prepared for Office of University Research, U.S. DOT, Washington, DC, September 1977.

27. Limbert, D. A., Richardson, H. H. and Wormley, D. N., "Dynamics and Control of Combined Lift-Guidance Ferromagnetic Vehicle Suspensions," Journal of Dynamic Systems, Measurement, and Control, ASME Transactions, Series G, Vol. 101, No. 3, September 1979.

28. Grunwald, K. J. and Johnson, W. G., "Aerodynamic Characteristics of Air-Cushion Models at Very Low Ground Clearances and at Freestream Dynamic Pressures Exceeding Cushion Pressure," NASA TN D-6011, NASA Langley Research Center, Hampton, VA, October 1970.

29. Hammitt, A. G., "The Aerodynamics of High-Speed Ground Transportation," Western Periodicals Co., North Hollywood, CA, 1973.

30. Ruetenik, J. R., and Zartarian, G., "Development of Methods for Predicting Airloads on TACV Configurations Due to Strong Crosswind Gusts," Report No. DOT-TSC-171-1 Kaman AviDyne, Burlington, MA, Prepared for Transportation Systems Center, Department of Transportation, Cambridge, MA, March 1972.

31. Ruetenik, J. R., "Correlation of Side-Force and Yawing Moment Data for TACV Configurations at Large Angles of Sideslip," Report No. FRA-ORD&D-74-29, Kaman AviDyne Division, Kaman Sciences Corporation, Burlington, MA, Prepared for Urban Mass Transportation Administration, USDOT, Washington, DC, January 1974.

32. A Cost Comparison of Three Tracked Air Cushion Configurations, Tracked Hovercraft Limited, London, England, Report No. FRA-RT-71-68, Prepared for Federal Railroad Administration, USDOT, Washington, DC, July 1970.

33. Neppert, H. and Sanderson, R., "Studies on the Aerodynamics of High Speed Trains," Translated from German by Information Company of America, Philadelphia, PA, Paper Presented at Symposium, at Hamburg, Germany, March 5, 1974.

34. Simley, R. F. and Ruetenik, J. R., "Calculations of Airloads on the Prototype TACV Configuration Due to Strong Crosswind Gusts," Report No. Kaman AviDyne TM-74, Kaman AviDyne Division, Kaman Sciences Corporation, Burlington, MA, Prepared for Transportation Systems Center, USDOT, Cambridge, MA, December 1973.

35. Bryson, A.E., Symmetric Vortex Separation on Circular Cylinders and Cones, Journal of Applied Mechanics, pp. 643-48, December 1959.

36. DYSYS-Operational Manual, Department of Mechanical Engineering, Massachusetts Institute of Technology, Cambridge, MA, July 1979.